AD-A031 103 STANFORD RESEARCH INST MENLO PARK CALIF F/G 17/9
DNA PROJECT 609 RADAR: AURORAL BACKSCATTER MEASUREMENTS.(U)
FEB 76 R T TSUNODA, R I PRESNELL, T N WANG DNA001-72-C-0179
UNCLASSIFIED DNA-3929F NL

1 OF 1
AD A031103

END

DATE FILMED
11-76

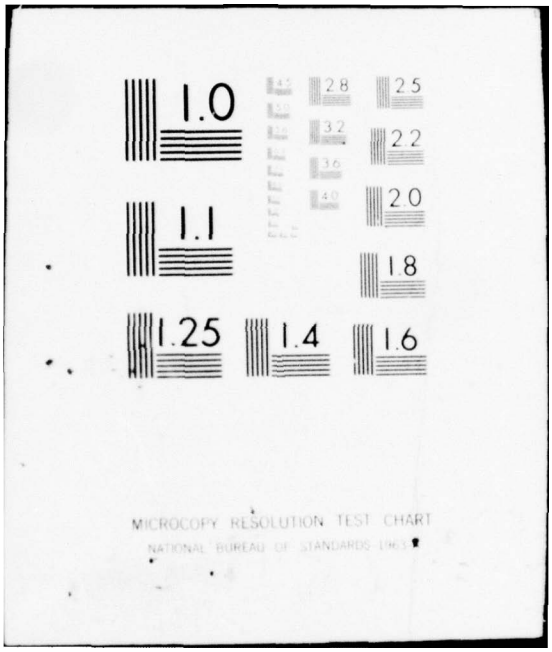
1.0
2.8
2.5
3.2
2.2
3.6
4.0
2.0
1.8
1.1
1.25
1.4
1.6
MICROCOPY RESOLUTION TEST CHART
NATIONAL BUREAU OF STANDARDS 1963

(12) A

DNA 3929F

DNA PROJECT 609 RADAR: AURORAL BACKSCATTER MEASUREMENTS

Stanford Research Institute
333 Ravenswood Avenue
Menlo Park, California 94025

February 1976

Final Report for Period 31 January 1974—30 September 1975

CONTRACT No. DNA 001-72-C-0179

THIS WORK SPONSORED BY THE DEFENSE NUCLEAR AGENCY
UNDER SUBTASK L25AAXHX631-07.

Prepared for

Director
DEFENSE NUCLEAR AGENCY
Washington, D. C. 20305

Destroy this report when it is no longer needed. Do not return to sender.

UNCLASSIFIED

SECURITY CLASSIFICATION OF THIS PAGE (When Data Entered)

REPORT DOCUMENTATION PAGE

READ INSTRUCTIONS BEFORE COMPLETING FORM

1. REPORT NUMBER: DNA 3929F	2. GOVT ACCESSION NO.
3. RECIPIENT'S CATALOG NUMBER	
4. TITLE (and Subtitle): DNA PROJECT 609 RADAR: AURORAL BACKSCATTER MEASUREMENTS	5. TYPE OF REPORT & PERIOD COVERED: Final Report, for Period 31 Jan 74—30 Sep 75
	6. PERFORMING ORG. REPORT NUMBER: SRI Project 2001
7. AUTHOR(s): R. T. Tsunoda, R. I. Presnell, T. N. C. Wang	8. CONTRACT OR GRANT NUMBER(s): DNA 001-72-C-0179
9. PERFORMING ORGANIZATION NAME AND ADDRESS: Stanford Research Institute, 333 Ravenswood Avenue, Menlo Park, California 94025	10. PROGRAM ELEMENT, PROJECT, TASK AREA & WORK UNIT NUMBERS: NWET-Subtask L25AAXHX631-07, SRI-2001
11. CONTROLLING OFFICE NAME AND ADDRESS: Director, Defense Nuclear Agency, Washington, D.C. 20305	12. REPORT DATE: Feb 76
	13. NUMBER OF PAGES: 54 (52 p.)
14. MONITORING AGENCY NAME & ADDRESS (if different from Controlling Office): X631	15. SECURITY CLASS. (of this report): UNCLASSIFIED
	15a. DECLASSIFICATION/DOWNGRADING SCHEDULE

16. DISTRIBUTION STATEMENT (of this Report)

Approved for public release; distribution unlimited.

DDC RELEASED OCT 22 1976

17. DISTRIBUTION STATEMENT (of the abstract entered in Block 20, if different from Report)

18. SUPPLEMENTARY NOTES

This work sponsored by the Defense Nuclear Agency under Subtask L25AAXHX631-07.

19. KEY WORDS (Continue on reverse side if necessary and identify by block number)

Ionospheric Physics	Ionospheric Electric Fields
Auroral Radar Clutter	Ionospheric Motions
Phased-array Radar	Electrojet Currents
Auroral Ionosphere	Auroral Storms

20. ABSTRACT (Continue on reverse side if necessary and identify by block number)

In this report we summarize the research results obtained from auroral backscatter studies using the DNA 609 radar system located at Homer, Alaska. The primary purpose of the backscatter studies was to improve our understanding of the auroral-clutter-producing mechanism. Most of the results are based on coordinated experiments utilizing the 398-MHz phased-array radar at Homer, the SRI/DNA incoherent-scatter radar at Chatanika, and other complementary auroral measurement techniques. We have found that the

DD FORM 1 JAN 73 1473 EDITION OF 1 NOV 65 IS OBSOLETE

UNCLASSIFIED

SECURITY CLASSIFICATION OF THIS PAGE (When Data Entered)

332 500

20. ABSTRACT (Continued)

problem can be most effectively approached by seeking both microscale and macroscale relationships--i.e., the relationships of local plasma parameters within the radar scattering volume producing auroral clutter, and the relationships of the large-scale auroral and magnetospheric conditions to the spatial distribution of auroral clutter, respectively. The results include the following:

(1) Diffuse auroral clutter is apparently not produced by primary plasma waves generated by the Buneman-Farley two-stream instability.

(2) The mechanism does not, however, appear to be unlike the quasi-linear gradient-drift instability model proposed by Sudan et al. (1973), which can be driven by the primary two-stream waves.

(3) There is a threshold electric field strength of 30 mV/m associated with the occurrence of 398-MHz diffuse auroral clutter.

(4) The diffuse auroral clutter is closely associated with the auroral electrojets.

(5) The evening diffuse auroral clutter is closely associated with downward field-aligned currents.

(6) Discrete auroral clutter is closely associated with the discrete visual aurora.

In addition to the above results, we present (1) a brief data summary taken in support of the DNA ICECAP '74A rocket program; (2) a description of the near-on-line Doppler capability that was added to the phased-array-radar system; (3) a discussion of a field trip to search for plasma-line backscatter associated with auroral activity; and (4) the current status of a theoretical study considering the ion-cyclotron instability as a contributor to the production of auroral clutter. Finally, we discuss the need for future studies of the characteristics of F-region auroral clutter, a phenomenon that has received little or no attention in the past. This type of auroral clutter has recently received theoretical support in the form of a plasma microinstability model.

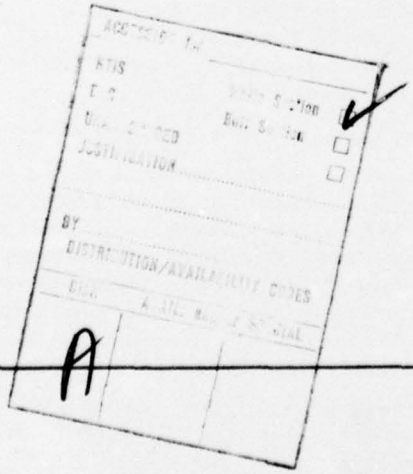

CONTENTS

ILLUSTRATIONS

I INTRODUCTION

DNA Project 609 originated in the fall of 1961. At that time, the design and construction of clutter radars was started in preparation for the FISH BOWL nuclear test series the following year. Following that test series, the radars were moved to Homer, Alaska to conduct auroral clutter studies. The radar system at that time consisted of six operational frequencies--50, 139, 398, 850, 1210, and 3000 MHz--all of which were transmitted and received through a common 60-ft parabolic dish antenna. The research results of past studies have been published in a number of Project 609 final reports.[1,2*]

In 1970, the design of the 398-MHz phased-array antenna system was started. The array was first assembled and tested at Stanford, California during 1972. The array was then disassembled, shipped, reassembled, and integrated with the 398-MHz radar system at Homer, Alaska. The first operation of the phased-array radar in an auroral environment was conducted during the spring of 1973.

It became immediately obvious from the first operation that the phased-array radar provided a quantum jump forward in our ability to unravel the lingering problems concerning the interpretation of auroral clutter-producing mechanisms. By the radar's rapid-scan capability and on-line computer support, the spatial distribution of auroral clutter, with minimal temporal/spatial ambiguities, could be mapped over a large

---

*References are listed at the end of this report.

geographical area. From these maps, true clutter boundaries (and their dynamics) could be discerned that were related to auroral and magnetospheric processes, and that were not due to radar characteristics.

Equally important was the installation of the Chatanika incoherent-scatter radar[3] beneath the central region scanned by the Homer radar. With the Chatanika radar, plasma parameters such as the electric field, electron density, and current density could be measured within the Homer radar scattering volume. With this combination, complemented by other auroral measurement techniques (e.g., all-sky cameras, magnetometers, and rocket-borne and satellite-borne instrumentation), great strides have been made toward an understanding of the auroral-clutter-producing mechanism.

The first research results using the 1973 data were presented in the most recent Project 609 final report.[4] Since then, several more field experiments have been conducted. Data analysis was continued on both the 1973 data and those collected during the subsequent field experiments. The research results covering the time period from 31 January 1974 to 30 September 1975 are the principal subject of this report. Details of the various studies conducted under this project have been published in the following journal articles:

- Tsunoda, R. T., R. I. Presnell, and R. L. Leadabrand, "Radar Auroral-Echo Characteristics as Seen by a 398-MHz Phased-Array Radar Operated at Homer, Alaska," J. Geophys. Res., 79, p. 4709, 1974.

- Wang, T. N. C. and R. T. Tsunoda, "On a Crossed Field Two-Stream Plasma Instability in the Auroral Plasma," J. Geophys. Res., 80, p. 2172, 1975.

- Hunsucker, R. D., G. J. Romick, W. L. Ecklund, R. A. Greenwald, B. B. Balsley, and R. T. Tsunoda, "Structure and Dynamics of Ionization and Auroral Luminosity During the Auroral Events of March 16, 1972, near Chatanika, Alaska," Radio Sci., 10, p. 813, 1975.

2

- Tsunoda, R. T., "Electric Field Measurements Above a Radar Scattering Volume Producing 'Diffuse' Auroral Echoes," J. Geophys. Res., 80, p. 4297, 1975.

- Tsunoda, R. T., "Doppler Velocity Maps of the Diffuse Radar Aurora," J. Geophys. Res., 81, in press, 1976.

- Tsunoda, R. T. and R. I. Presnell, "On a Threshold Electric Field Associated with the 398-MHz Diffuse Radar Aurora," J. Geophys. Res., 81, p. 88, 1976.

- Tsunoda, R. T., R. I. Presnell, and T. A. Potemra, "The Spatial Relationship Between the Evening Radar Aurora and Field-Aligned Currents," J. Geophys. Res., 81, in press, 1976.

- Tsunoda, R. T., R. I. Presnell, Y. Kamide, and S. -I. Akasofu, "Relationship of Radar Aurora, Visual Aurora, and Auroral Electrojets in the Evening Sector," submitted to J. Geophys. Res., 1976.

Papers in preparation include:

- Wang, T. N. C. and R. T. Tsunoda, "The Effects of Field-Aligned Gradients on the Two-Stream Instability in an Auroral Plasma."

- Brekke, A., R. T. Tsunoda, and M. J. Baron, "On the Azimuthal Dependence of Slant Range Doppler Shift."

Because most of the research results have appeared or will appear in the open literature, we present only a summary of the results. The results of the data analysis are presented in Section II. A description of field experiments (in particular, support of the DNA ICECAP '74 rocket program) and any additions, improvements, or modifications to the radar system are described in Section III. The results of theoretical studies evaluating the ion-cyclotron instability as a possible source of auroral clutter are presented in Section IV. A discussion of the results is presented in Section V. And finally, conclusions and recommendations for further studies are presented in Section VI.

II DATA ANALYSIS

In the study of auroral-clutter-producing mechanisms, we have found that the problem is most effectively approached by seeking both "microscale" and "macroscale" relationships. By microscale, we refer to the local conditions within the radar scattering volume that seem to determine the behavior of auroral clutter. In particular, we were most interested in plasma parameters such as the electric field, current density, electron density, etc. within the radar scattering volume, and their relationship to auroral clutter characteristics. And by macroscale, we refer to the large-scale auroral and magnetospheric conditions that appear to be associated with the spatial distribution of auroral clutter. In particular, we were most interested in relating the spatial distribution of the convection electric field, particle precipitation, auroral electrojets, field-aligned currents, visual aurora, etc., to the spatial distribution of auroral clutter. Furthermore, by comparing the macroscale relationships with microscale relationships, we were able to derive a consistent phenomenology from which we can more intelligently interpret the auroral clutter characteristics, particularly under complex and dynamic conditions.

A. Microscale Relationships

Comprehensive microscale studies of auroral clutter characteristics were made possible by the installation of the incoherent-scatter radar at Chatanika, Alaska.[3] The locations of the Homer and Chatanika radars are shown on a map of Alaska in Figure 1. Chatanika is situated directly beneath the central region scanned by the Homer radar (shown by a pie-

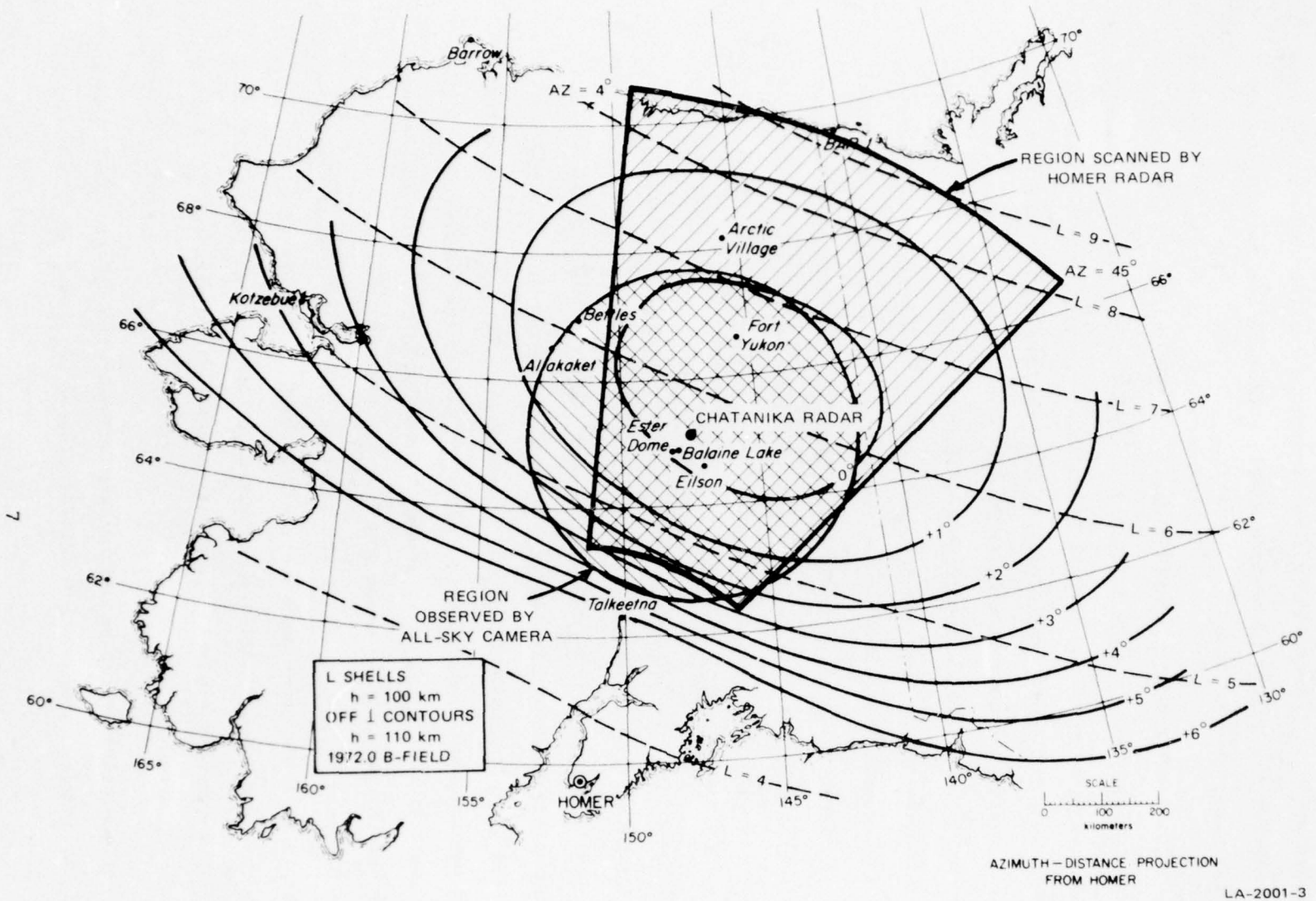

FIGURE 1 LOCATIONS OF THE HOMER AND CHATANIKA RADARS

shaped sector). Consequently, the incoherent-scatter radar can be used to monitor the plasma parameters within and/or in the vicinity of the Homer radar scattering volume.

The first coordinated study using the two radars was conducted in 1972 and the results were published in a Chatanika radar final report[5] and subsequently as two journal papers.[6,7] The approach taken in that study was to compare the auroral clutter characteristics with the electric field vector and neutral wind determined from Chatanika radar measurements.[8,9] The first significant result was the finding that "diffuse" auroral clutter[4,10] was not produced by primary plasma waves generated by the Buneman-Farley two-stream instability.[11,12] However, the electric field strength was found to be large enough so that the two-stream instability was operative. In other words, while primary plasma waves were present, they were not responsible for the backscatter observed over the azimuth sector scanned by the Homer radar. From the analysis of the Doppler spectra of auroral clutter, we concluded that diffuse auroral clutter may be associated with secondary plasma waves generated by the same instability. An alternative interpretation is that these secondary waves could be produced by the gradient-drift instability[13] driven by the primary two-stream plasma waves. The interaction between the two instabilities, which is accounted for in the quasi-linear plasma instability model, was first proposed by Sudan et al.[13] and applied to the auroral geometry by Greenwald.[14] The interaction was suggested by the observed Doppler velocity and its apparent dependence on the angle made between the radar beam and the direction of current flow. Finally, the analysis[6] showed that the occurrence of auroral clutter at 398 MHz might be associated with a threshold electric field strength of approximately 30 mV/m.

The possible relationship between ionospheric electric field strength and the occurrence of diffuse auroral clutter was confirmed and presented

in the previous Project 609 Final Report[4] and in a paper by Tsunoda and Presnell.[15] With the 398-MHz phased-array radar, diffuse auroral clutter was found to occur over Chatanika whenever the measured ionospheric electric field strength exceeded a nominal value of 30 mV/m. When the electric field strength was less than that value, auroral clutter was not observed, regardless of the electron density. The threshold value is consistent with the activation of the two-stream instability as the primary driving mechanism.

B. Macroscale Relationships

The first results of this kind were obtained through analysis of the Spring 1973 data and reported in the previous final report[4] and in a paper on the first phased-array radar results.[10] We showed that auroral clutter displayed a consistent morphology based on spatial distribution of the ionospheric electric field and the E-region electron density. The requirement of both an electric field and an electron density clarified the hitherto puzzling relationship between auroral clutter and the visual aurora.[1] The diffuse auroral clutter that occasionally extends over several hundreds of kilometers in latitude was found in the evening sector to be located equatorward of the most equatorward visual arc. This result is apparently due to (1) subthreshold electric field strengths associated with regions of intense precipitation, and/or (2) the absence of significant particle precipitation in regions poleward of the diffuse auroral clutter and distant from the locations of the visual arcs.

The second interpretation is supported in another study[16] comparing the spatial distributions of auroral clutter, auroral electrojets and visual aurora. The eastward electrojet (as determined by a meridian chain of magnetometers) was found to be collocated with the diffuse auroral clutter. In fact, the boundaries of diffuse auroral clutter could be used to define boundaries of the eastward electrojet. These results are

consistent with the findings of Greenwald et al.[17,18] for 50 MHz, that the range-integrated backscatter amplitude is often linearly proportional to the horizontal perturbation component $\sqrt{(\Delta H)^2 + (\Delta D)^2}$ of the geomagnetic field. The occurrence of the eastward electrojet (and diffuse auroral clutter) in a region equatorward of the discrete visual aurora is consistent with the presence of large electric fields in regions of diffuse particle precipitation.[19]

In the morning sector, both diffuse and structured complex auroral clutter were associated with the regions containing visual aurora. The difference in the spatial correlation of auroral clutter with visual aurora implies that the electric field strength is not depressed or small within visual forms that occur in the morning sector. Auroral arc models that allow polarization fields to exist within arcs and in which the westward electric field drives a Pedersen current appear to be consistent with the data.[20]

In another study,[21] we found that the diffuse auroral clutter in the evening sector, which was found to be collocated with the eastward electrojet, was also collocated with the region containing downward field-aligned currents. The field-aligned currents were detected by a vector magnetometer onboard the Navy/APL TRIAD satellite. The collocation of field-aligned currents with auroral clutter suggests that plasma instabilities driven by such currents must be considered as possible contributors to the production of auroral clutter. For this reason, a theoretical study of the ion-cyclotron instability was initiated. The first results of that study are presented in Section IV.

The relationships discussed above can be used to interpret what is now believed to be a typical evening-sector case under moderately disturbed conditions. An example is shown in Figure 2. The 40^{o} azimuth sector typically scanned by the Homer radar is seen to contain the two

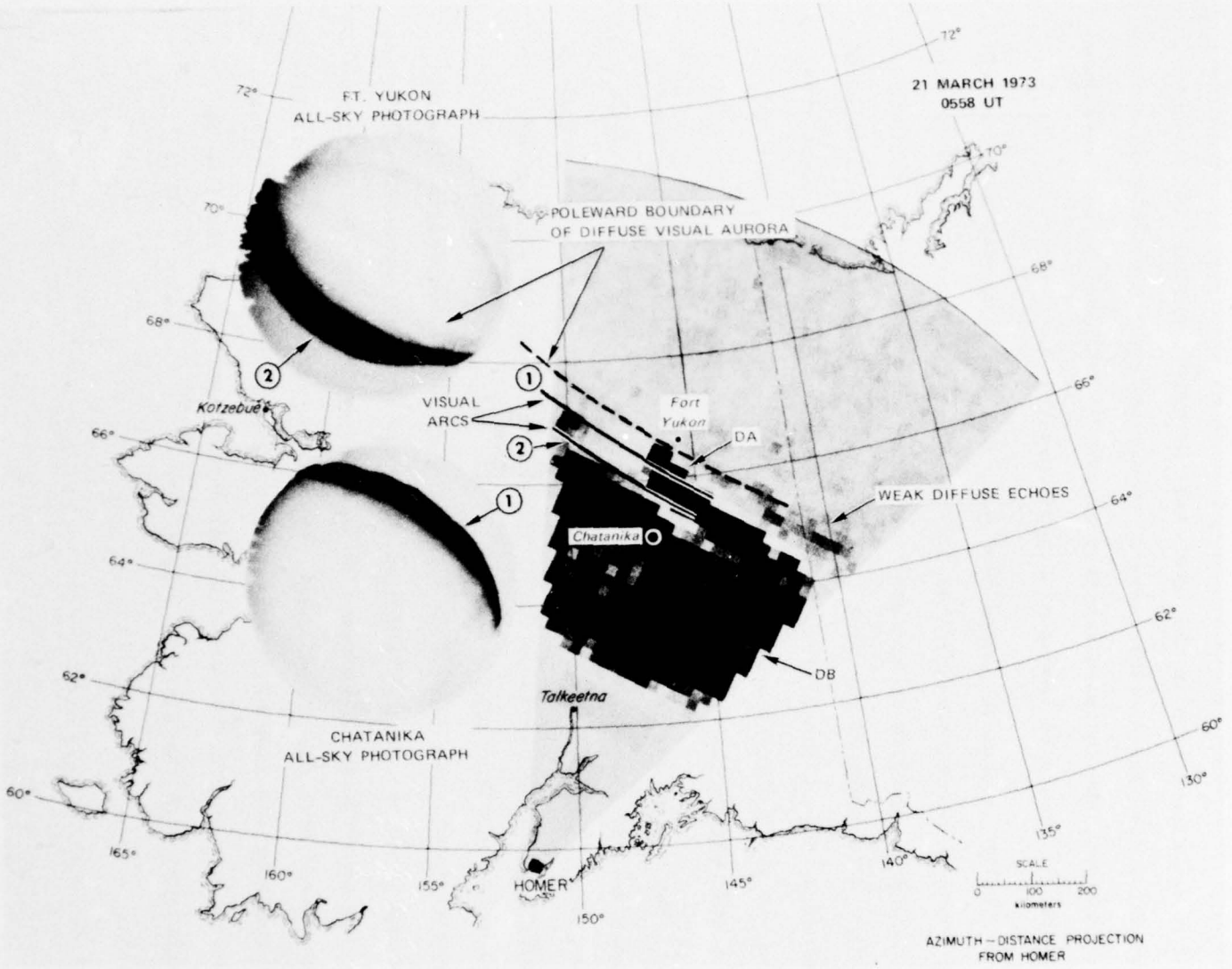

FIGURE 2 EXAMPLE OF SPATIAL MAP OF THE RADAR AURORA, 21 MARCH 1973

basic types of auroral clutter, the diffuse band (DB), and the discrete arc (DA).[4,10] Visual arcs scaled from all-sky-camera (ASC) photographs taken at Fort Yukon and Chatanika are shown as solid lines. (A third, faint visual arc seen in the upper half of the Fort Yukon ASC photograph was not scaled because there was no corresponding auroral clutter feature.) In addition, the poleward boundary of what is believed to be the diffuse aurora[22,23] has also been scaled and shown as a dashed line.

The DB is seen to extend from just north of Talkeetna (and limited by magnetic aspect sensitivity) to almost directly over Fort Yukon. The DB poleward boundary is assumed, in this case, to correspond to the poleward boundary of the weak diffuse echoes that is coincident with the poleward edge of the diffuse visual aurora. If this is the case, the two visual arcs and the DA, which is situated between them, must be imbedded within the DB.

The morphology is consistent with that found from scanning photometer data taken from the ISIS-2 satellite.[22,23] The discrete auroral arcs are imbedded within but near the poleward boundary of the region of diffuse particle precipitation. The DB corresponds to a region of enhanced electric field strength, diffuse particle precipitation, downward field-aligned current flow, and the eastward electrojet. The DB is modulated near its poleward boundary due to a corresponding modulation in the electric field produced by intense localized particle precipitation associated with the visual arcs. The DB poleward boundary is therefore produced by the absence of significant particle precipitation poleward of the diffuse aurora. Upward field-aligned currents were found to be associated with the discrete visual arcs.[16,24]

III FIELD EXPERIMENTS

A. ICECAP '74

Two field trips were made, to participate in the DNA ICECAP '74A and '74B rocket programs. The Homer radar was operated between February 13 and March 2 during the '74A rocket launches from the Poker Flat rocket range and between April 5 and 19, the time period of the '74B rocket program. However, due to on-line computer difficulties, no auroral clutter data were collected during the times of the ICECAP '74B rocket launches. Approximately 46 hours of clutter-map data were collected during the two field operations. In the following subsections, we present a brief summary of the Homer radar data collected during the time periods around the ICECAP '74A rocket launches.

1. 14 February 1974--Black Brant and Ute Tomahawk

A Black Brant rocket (A18.006-4) carrying instrumentation to measure IR spectra during quiet conditions was launched from Poker Flat at 0607 UT. Thirty-seven minutes later, a Ute-Tomahawk rocket was also launched, carrying instrumentation to determine the neutral atmospheric density and temperature, also during quiet conditions. The geomagnetic and auroral conditions during this time period were relatively quiet,[25] with the College H-component only about 10γ above the quiet-time level. Any visual auroral activity that may have been over Chatanika was obscured by clouds.

Auroral clutter was first seen around 0555 UT approximately 300 km northeast of Chatanika. The echoes were relatively limited in both latitudinal and longitudinal extent, in contrast to the broad

diffuse-band (DB) signatures[4,10] that are often seen during this time period under more active auroral conditions (see Figure 2). By the time of the rocket launch, the DB had moved within 200 km north of Chatanika (and directly over Fort Yukon), but had also weakened. An auroral clutter map taken around two minutes after launch is shown in Figure 3. The DB is seen to be patchy but can be shown to be more or less aligned along a constant magnetic L-shell. The DB can be seen, by exercising a little imagination, to be bifurcated. That is, there appears to be a region within the DB where no auroral clutter is observed. That region also appears to be aligned along an L-shell. The auroral clutter continued to weaken and was essentially gone by 0606 UT.

Peak electron densities measured by the Chatanika radar were typically less than 5×10^4 el/cm^3 in the E region and no higher than 10^5 el/cm^3 in the F layer.[25] Since the returned incoherent-scatter power was so small, reliable estimates of the electric field could not be made.

Tsunoda and Presnell[15] showed that in addition to a threshold electric field strength of 30 mV/m, there was a minimum electron density below which diffuse auroral clutter also could not be detected. That value was a few parts times 10^4 el/cm^3. While it was not established whether the minimum electron density represented a true "threshold" in the electron density or whether it corresponded with the sensitivity threshold of the radar, the low E-region electron density measured by the Chatanika radar implies that the electric field strength could have been greater than 30 mV/m. If this is the case, the presence of bifurcated DB over Fort Yukon may be due to the presence of an auroral arc in the region of no radar echo. The auroral arc corresponds in location to a region of localized particle precipitation, and hence, enhanced electron density. The absence of auroral clutter within the bifurcated region could be explained by the depression of the electric field (in the evening sector) by the intense ionization.[15] This question can be answered by

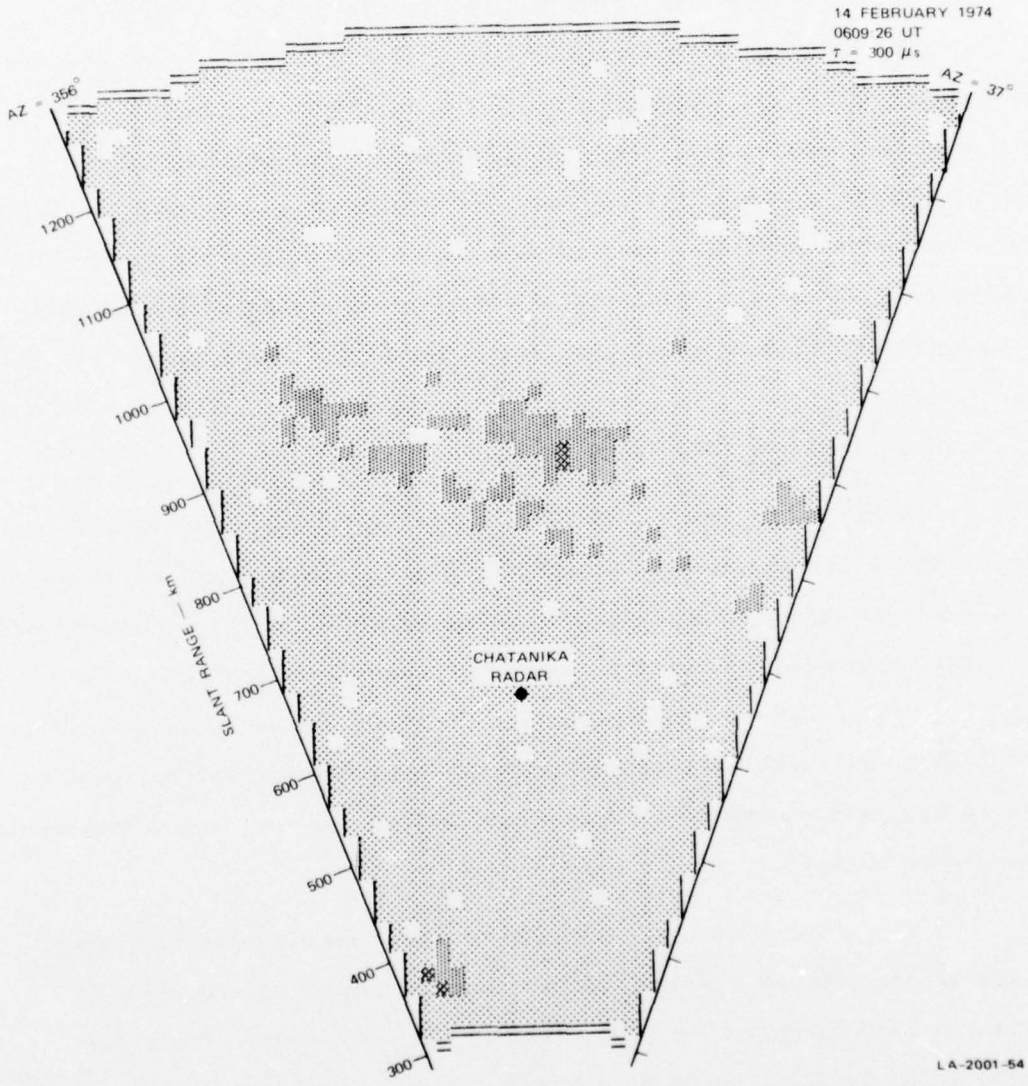

FIGURE 3 REAL-TIME SECTOR SCAN — 14 FEBRUARY 1974, 0609:26 UT

referring to optical (either all-sky or photometer) data taken from Fort Yukon. Based on the findings presented in Tsunoda et al.,[16] that visual arc, if present, is probably located near the lower latitudinal boundary of the Harang discontinuity.[26]

The second rocket was launched at 0644 UT during quiet magnetic conditions that persisted from the first rocket launch. The auroral clutter continued to be very weak and patchy since their reappearance around 0640 UT. The auroral clutter map corresponding to approximately two minutes after the second rocket launch is shown in Figure 4. The echoes at around 900 km in the east azimuths may be remnants of the DB seen around the first rocket launch. The isolated echo patches south of Chatanika and seemingly aligned along a magnetic latitude may be related to a visual arc, although all-sky-camera photographs available from Chatanika did not reveal any aurora due to continued cloud coverage.

2. 19 February 1974--Nike Hydac

A Nike-Hydac rocket (NH 74-1) carrying a TMA chemical release payload and a falling-sphere atmospheric density experiment was launched at 0744 UT during quiet conditions. Geomagnetic activity at College was low, although some perturbation began just prior to launch at about 0720 UT.[25] The magnetic deflections can be interpreted in terms of the development of a weak westward current, located poleward of College. This current system was localized, since Barrow did not record substantial geomagnetic activity.

The auroral clutter, similar to those seen during the first rocket launch, formed a weak DB approximately 200 km northeast of Chatanika (and directly over Fort Yukon). Shortly before the rocket launch (0742:30 UT), the DB bifurcated into two latitudinal segments, possibly due to the development of a visual arc within the DB. (A faint

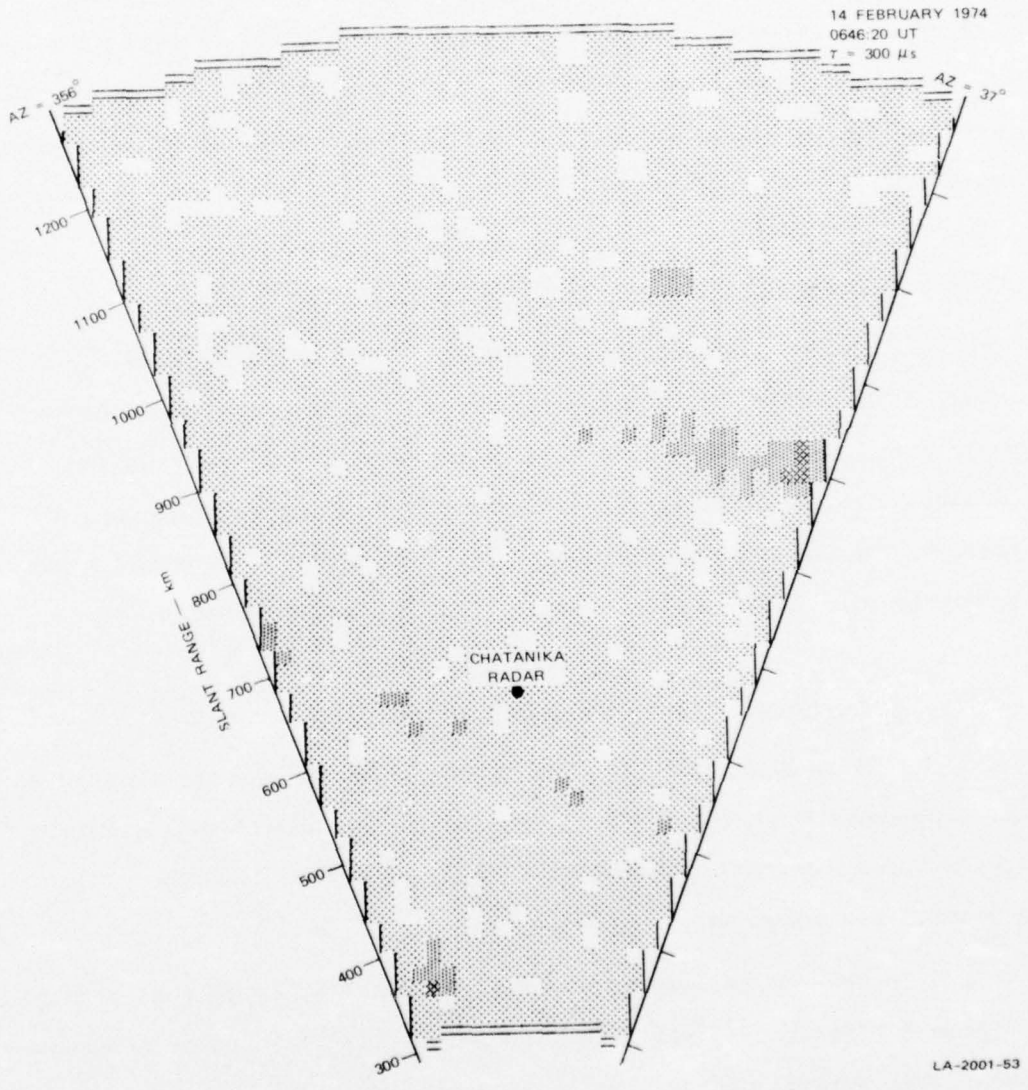

FIGURE 4 REAL-TIME SECTOR SCAN — 14 FEBRUARY 1974, 0646:20 UT

auroral arc was observed on the northern horizon of the Chatanika all-sky-camera photograph and also by a meridian-scanning 5577-Å photometer operated by AFCRL/USU.[25]) The auroral clutter map taken approximately two minutes after the rocket launch is shown in Figure 5. By this time, the echoes had weakened, becoming patchy.

The electron densities were very low, as measured by the Chatanika radar.[25] The E-region electron density was approximately 10^4 el/cm^3, again leaving open the possibility that the electric field could have been greater than 30 mV/m. The F-region electron density was no greater than 0.7×10^4 el/cm^3, determined only after 43 minutes of integration.

3. 21 February 1974--Black Brant (HIRIS)

A Black Brant rocket (A18.116-1) with a HIRIS payload was launched at 0916:30 UT during active auroral and geomagnetic conditions.[25] Unfortunately, during this time period the Homer phased-array radar developed software difficulties associated with the electronic scanning. Auroral clutter data were, however, collected on the 139-MHz radar but will not be presented due to difficulty in its interpretation.

4. 25 February 1974--Black Brant (MULTI)

A Black Brant rocket (A18.219-1), carrying a MULTI payload to observe upper-atmospheric chemical processes and IR emissions within a bright auroral arc, was launched at 0738:30 UT during disturbed auroral and geomagnetic conditions.[25]

The characteristic DB radar signature similar to that presented in Figure 2 (Section II) was seen throughout this time sector around the launch. The auroral clutter map taken approximately two minutes after

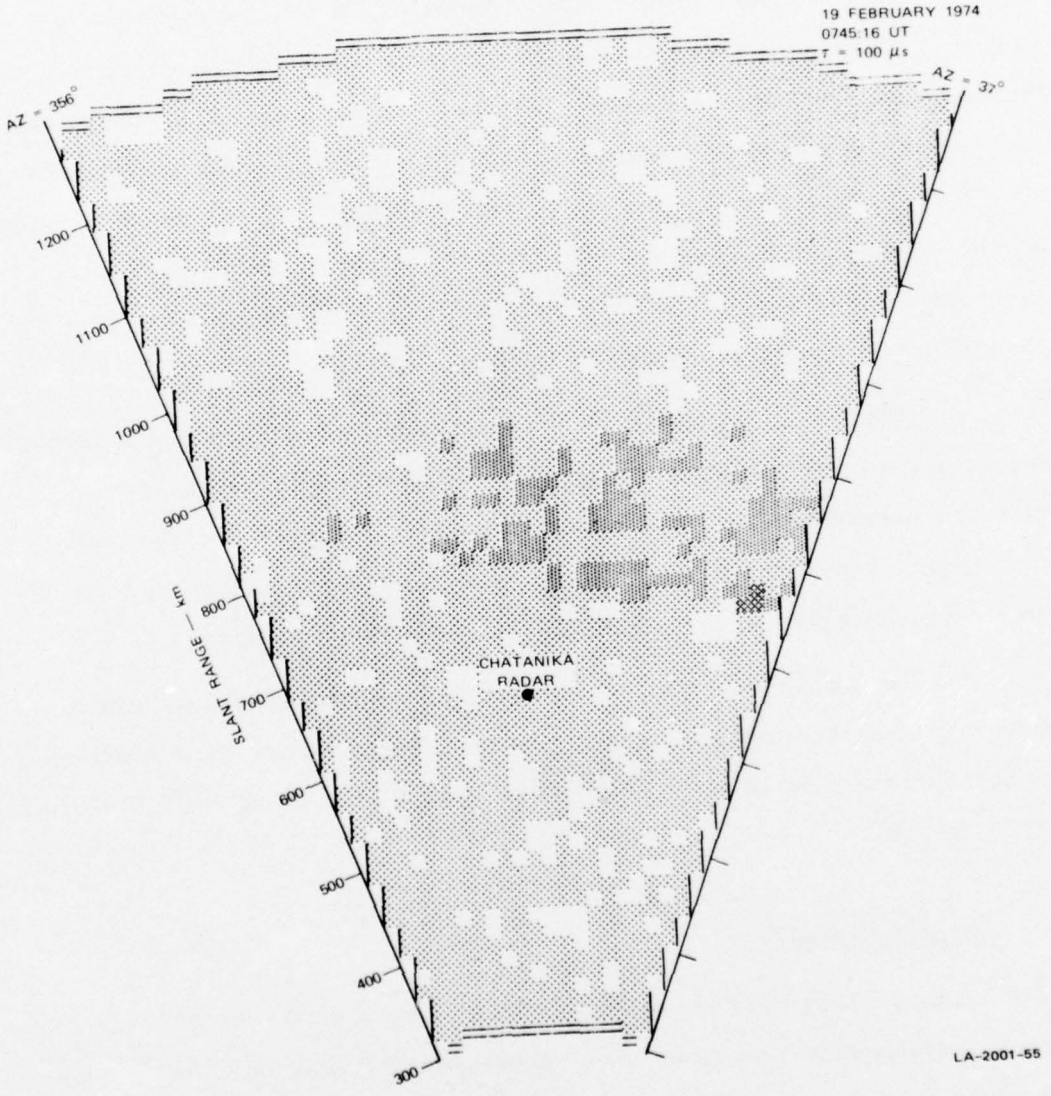

FIGURE 5 REAL-TIME SECTOR SCAN — 19 FEBRUARY 1974, 0745:16 UT

the rocket launch is shown in Figure 6. The map format was changed from the polar-plot format shown in the first three figures to the rectangular slant-versus-azimuth format, due to on-line difficulties with the polar-plot format.

The DB is seen to extend from 50 km north of Chatanika to approximately 200 km south of Chatanika where the auroral clutter is cut off by magnetic aspect sensitivity. Examination of Chatanika all-sky-camera photographs showed that a bright visual arc was located along the DB poleward boundary. A second, faint arc segment was also seen directly over and to the west of Chatanika that coincides with the bifurcation in the DB over Chatanika (Figure 6). The bifurcation was apparently produced by the depression of the electric field by particle precipitation. A westward-traveling surge passed over Chatanika within the next five minutes along the DB poleward boundary.

The DB is typical of that usually observed during a moderately active evening period when the DB is essentially collocated with the eastward electrojet and the poleward boundary representing the lower latitudinal boundary of the Harang discontinuity. Furthermore, the DB represents a region of downward field-aligned current flow.

In accord with the above description, the Chatanika radar measured a northeastward-directed electric field vector with a strength of approximately 60 mV/m. E-layer electron densities were of the order of 10^5 el/cm^3.

B. Doppler Capability

A third field trip was made during November 1974 to install a hard-wired fast-Fourier-transform (FFT) processor for near on-line spectral observations of auroral clutter. The computer programming necessary to operate the clutter-mapping radar and to take data in a desired format

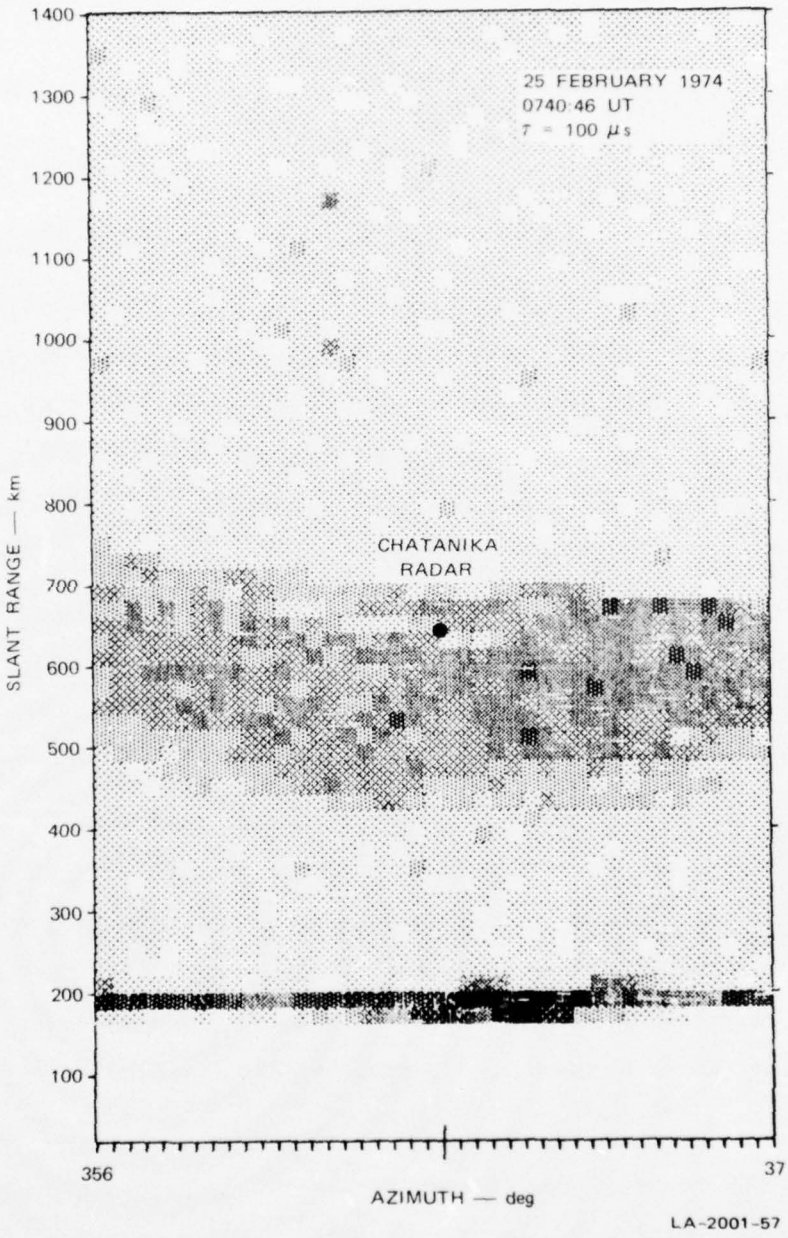

FIGURE 6 REAL-TIME B-SCAN — 25 FEBRUARY 1974, 0740:46 UT

was completed and debugged. The programming necessary to process the prerecorded clutter data through the FFT processor and to plot Doppler-velocity maps was also completed. In the process of debugging this latter program, it was found that the FFT processor would not execute transforms at the required rate. At the end of the field trip, this processor was returned to the SRI Menlo Park facility. Approximately 12 hours of clutter Doppler data were recorded during the field trip.

To see if the data had been recorded properly, a data set collected during a period of substorm activity (1128 UT, 20 November 1974) was processed using software FFT techniques. The results are shown in Figure 7. The on-line auroral clutter map is shown in Figure 7(a). In order to accommodate the larger computer memory requirements, only the data from 400 km to 1100 km slant range are processed and mapped. The clutter map does not appear to reveal any complex echo structure that might be expected under substorm conditions. Auroral clutter is seen to extend from 450 km, where the radar echoes are cut off by magnetic aspect sensitivity, to 1100 km, where the clutter appears weaker and more patchy.

To minimize computation time, only the data taken every 2^{o} in elevation and 4^{o} in azimuth were processed. Contours of constant Doppler velocity were then hand-drawn through the mean Doppler-velocity values. The results, shown in Figure 7(b), are clearly more complex in velocity space than they are in clutter-amplitude space. There appears to be no obvious relationship between the observed radial Doppler velocities and clutter amplitude.

Other than the fact that the data were indeed recorded properly, little physics can be extracted from this particular example. Actual analysis and utility of the Doppler data will have to begin with more stable periods--e.g., those in which there exists a well-behaved afternoon or evening DB or stable discrete arcs (DA).

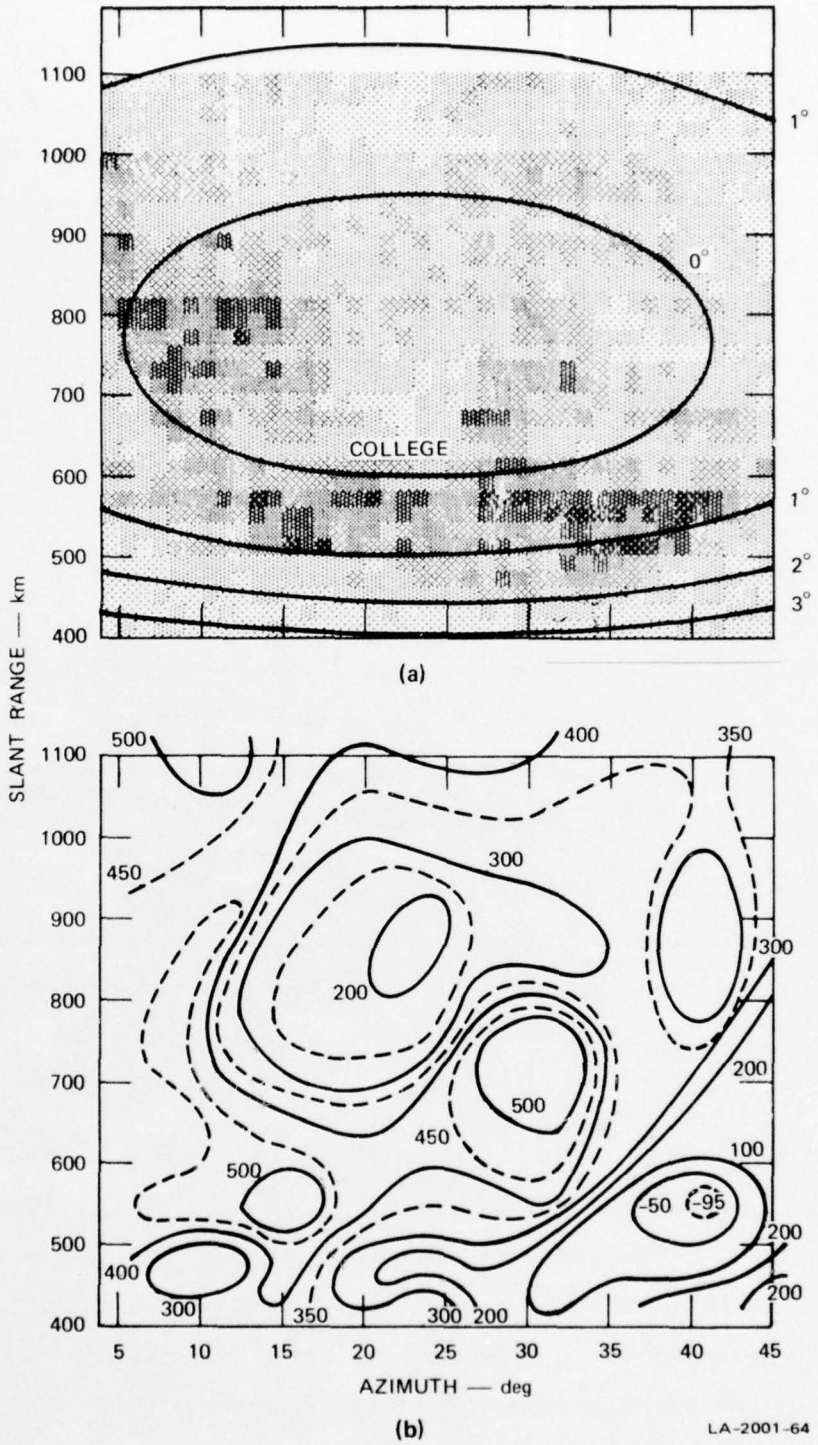

FIGURE 7 AURORAL CLUTTER MAP AND CORRESPONDING DOPPLER-VELOCITY MAP — 1128 UT, 20 NOVEMBER 1974

C. Search for Plasma Line Backscatter

A final field trip was made during 10-17 March 1975 to search for the possible existence of plasma-line backscatter during periods of intense auroral activity. This study was initiated by Dr. John Minkoff of Riverside Research Institute. Having participated in ionospheric RF heating experiments where plasma-line backscatter was observed,[27] Dr. Minkoff approached the National Science Foundation with a proposal, which was accepted, to search for the possible presence of plasma-line backscatter that might be associated with auroral activity.

The 139- and 398-MHz radars at Homer were operated using the 60-ft reflector antenna. A Hewlett-Packard spectrum analyzer was connected to the 30-MHz IF of one of the two radars. The analyzer allowed a search in frequency on both sides of the "on frequency" auroral clutter echo. Searches were made to ±10 MHz. A range gate was used to allow only the auroral clutter into the spectrum analyzer.

The operational procedure was to make a search for auroral clutter by manually scanning the antenna and using the normal A-scan display. After a large signal-to-noise ratio (SNR) echo was found, the manually controlled range gate was positioned on the auroral echo and the spectrum analyzer was used at both 139 and 398 MHz, alternately.

Over a period of six days this technique was used to search for plasma-line backscatter at all hours of the night and day. During the six days, both diffuse and discrete auroral echoes were observed with amplitudes up to 40 dB SNR. These signal strengths correspond to some of the strongest auroral clutter ever observed with the Homer radar. However, at no time were echoes observed off-channel at a frequency that might correspond to the plasma frequency. The search included not only the E layer with auroral clutter present, but the F layer above existing auroral clutter.

The negative results suggest at least two possibilities. First, if we assume that plasma-line backscatter is related to the amount of energy that is deposited, it can be shown through Chatanika radar measurements that Joule and particle heating are easily several orders of magnitude less than that produced by the RF heater used in the coherent heating experiments. And second, the fact that the aurora constitutes an incoherent source (i.e., broadband in frequency space) of energy suggests that sideband generation at a particular frequency--say, the plasma frequency--does not take place. Instead, any sideband generation, if present, may have a broadband distribution, similar to the input energy distribution, that is not intense enough to be detected at any particular frequency by an auroral backscatter radar. In this case, integration in frequency space (as well as in time) excluding the "on frequency" returns may reveal a detectable signal.

IV THE ION-CYCLOTRON WAVE AND ASSOCIATED INSTABILITIES

A. General

Recently D'Angelo[28] suggested that the Type III spectra associated with the radar aurora[29] may possibly be explained by unstable ion cyclotron waves. A number of previous works on the electron cyclotron waves indicate that field-aligned streams and currents can make the wave grow. It is expected that similar instabilities are also possible for the ion cyclotron waves. Recently, a large amount of experimental evidence has been presented confirming the presence of field-aligned current and streams in the auroral region. It is therefore important to investigate possible instabilities associated with ion cyclotron waves.

We have started to work on this problem during the current contract, but the work is not yet completed. At the present time, various forms of dispersion equations based on kinetic theory have been derived, and the propagation characteristics for the ion cyclotron waves in a stable plasma have been determined. These results are presented in this section.

B. Dispersion Equation

In a uniform, collisionless magnetoplasma, the dispersion equation for a quasi-static wave ($\vec{E} \parallel \vec{k}$) can be derived from the Vlasov and Poisson equations. The procedures are as follows: One first integrates the Vlasov equation along the orbit of the particles to obtain a charge expression for each species in terms of the wave field. Then the charge expression is substituted into Poisson's equation to eliminate the wave field and to obtain a dispersion equation. By assuming that only first-order perturbations are important, the Vlasov equation and Poisson's

equation, as well as the above derivation procedure, can be linearized. By this we mean that the perturbing wave field $\vec{E}$ is a first-order (small) quantity, and the particle distribution function can be written as $f = f_0 + f_1$, where f_0 is the equilibrium distribution, and f_1 is the first-order perturbed distribution due to $\vec{E}$. In the integration of the linearized Vlasov equation, the integration is performed along the orbit of the unperturbed particles.

While the procedure is as described above, we omit the lengthy algebra involved in the actual derivation and simply give the following general form of the dispersion equation:

$$D(\omega,\vec{k}) = 1 - \sum_s \frac{\omega_p^2}{k^2} \sum_{n=-\infty}^{\infty} 2\pi \int_{-\infty}^{\infty} dV_\parallel \int_0^{\infty} V_\perp dV_\perp \left[k_\parallel \frac{\partial f_0}{\partial V_\parallel} + \frac{n\omega_c}{V_\perp} \frac{\partial f_0}{\partial V_\perp} \right] \frac{J_n^2(\varkappa)}{\omega - k_\parallel V_\parallel - n\omega_c} \qquad (1)$$

where

ω_p = Plasma frequency

ω_c = Gyrofrequency

k = Wave number

$J_n(\varkappa)$ = n^{th}-order Bessel function of first kind

f_0 = Unperturbed particle distribution function

$\varkappa = k_\perp V_\perp / \omega_c$

n = Integer.

The subscripts "$\parallel$" and "$\perp$" stand for the components parallel to and perpendicular to the static magnetic field $\vec{B}_o$, respectively. $\sum_s$ stands for summing over all charged-particle species.

For the case of collisions, the Boltzman equation must be used to replace the Vlasov equation. However, the exact integral form of the rate of change of the distribution function due to the collisions is extremely

complicated. A usual approximation to that integral form is known as the BGK model, where the collisional integral in the Boltzmann equation is replaced by $\nu[f_0(1 + n_1/n_0) - f]$. Here, n_0 is the unperturbed particle density, n_1 is the first-order perturbed density, and ν is the effective collision frequency. The BGK collision model allows the particles to relax in position space to the local density, rather than to the unperturbed density n_0 which corresponds to f_0, and conserves particles in position space.

With the BGK model of collisions for each species taken into account, the derivation of the dispersion equation is similar to that for the collisionless case. It can be shown that the general form of the dispersion equation is again given by Eq. (1) after replacing ω_p^2 by

$$\omega_p^2 \left[1 - j(\nu/\omega)\right]$$

and replacing ω in $(\omega - k_\parallel V_\parallel - n\omega_c)$ by $(\omega - j\nu)$, where $j = \sqrt{-1}$.

While the general form of the dispersion equation is given above, we now proceed to reduce Eq. (1) for a number of specific unperturbed distribution functions.

1. Zero-Drift, Isotropic Maxwellian Distributions

The distribution functions for the electrons and ions take the form

$$f_o(\vec{V}) = \left(\frac{1}{2\pi U_t^2}\right)^{3/2} e^{-\frac{(V_\perp^2 + V_\parallel^2)}{2U_t^2}} \qquad (2)$$

where the subscripts for the electrons and ions are omitted and where U_t stands for the thermal speed.

Substituting Eq. (2) into Eq. (1) and performing the integrations in velocity space yields the dispersion equation:

$$k^2 + \sum_{e,i} k_\perp^2 \frac{\omega_p^2}{\omega_c^2} \sum_{n=-\infty}^{\infty} \frac{e^{-\lambda} I_n(\lambda)}{\lambda} \left[1 + \frac{\omega}{\sqrt{2}\, k_\parallel U_t} Z(\xi) \right] = 0 \qquad (3)$$

where $\lambda = (k_\perp U_t/\omega_c)^2$, $I_n(\lambda) = n^{th}$-order Bessel function of the third kind, and $Z(\xi)$ is known as the plasma dispersion function,[30] $\xi = (\omega - n\,\omega_c)/\sqrt{2}\, k_\parallel U_t$.

When the collisions are included, Eq. (3) becomes

$$k^2 + \sum_{e,i} k_\perp^2 \frac{\omega_p^2 (1 - j\frac{\nu}{\omega})}{\omega_c^2} \sum_{n=-\infty}^{\infty} \frac{e^{-\lambda} I_n(\lambda)}{\lambda} \left[1 + \frac{\omega - j\nu}{\sqrt{2}\, k_\parallel U_t} Z(\xi) \right] = 0 \qquad (4)$$

where ξ in Eq. (4) now becomes

$$\xi = \frac{\omega - j\nu - n\omega_c}{\sqrt{2}\, k_\parallel U_t} \quad .$$

2. Anisotropic, Zero-Drift Maxwellian Distributions

In this case the thermal velocity takes different component values in the directions parallel to and perpendicular to the static magnetic field. The Maxwellian distributions for the electrons and ions take the following form:

$$f_o(\vec{V}) = \frac{1}{(2\pi)^{3/2} U_\parallel U_\perp^2} e^{-\frac{V_\perp^2}{2U_\perp^2} - \frac{V_\parallel^2}{2U_\parallel^2}} \qquad (5)$$

where $U_{\parallel,\perp}$ stands for the thermal velocity parallel and perpendicular to $\vec{B}_o$, respectively.

Inserting Eq. (5) into Eq. (1) yields

$$k^2 + \sum_{e,i} k_\perp^2 + \frac{\omega_p^2}{U_\parallel^2}\frac{U_\perp^2}{\omega_c^2} \sum_{n=-\infty}^{\infty} \frac{e^{-\lambda} I_n(\lambda)}{\lambda} \left[1 + \frac{\omega - (1 - \frac{U_\parallel^2}{U_\perp^2})\, n\omega_c}{\sqrt{2}\, k_\parallel U_\parallel} Z(\xi) \right] = 0 \qquad (6)$$

where λ and ξ are now defined as

$$\lambda = \left(\frac{k_\perp U_\perp}{\omega_c}\right) \quad , \qquad \xi = \frac{\omega - n\omega_c}{\sqrt{2}\, k_\parallel U_\parallel} \quad .$$

In the limit of $U_\perp = U_\parallel = U_t$, Eq. (5) reduces to Eq. (2). It is clear that Eq. (6) becomes identical to Eq. (3).

For the case of collisions included, we simply replace ω_p^2 by $\omega_p^2(1 - j\frac{\nu}{\omega})$, and ω by $(\omega - j\nu)$, in Eq. (6) to obtain the new dispersion equation. In comparison with the dispersion equation derived by Tataronis and Crawford,[31] we point out that Eq. (19) of their paper appears to be incorrect.

3. Field-Aligned Drift Maxwellians

Let U_d be the drift velocity along $\vec{B}_o$; the distribution function is given by

$$f_0(\vec{V}) = \left(\frac{1}{2\pi U_t^3}\right)^{3/2} e^{-\frac{[V_\perp^2 + (V_\parallel - U_d)^2]}{2U_t^2}} \qquad (7)$$

and the dispersion equation [Eq. (3)] becomes

$$k^2 + \sum_{e,i} k_\perp^2 \frac{\omega_p^2}{\omega^2} \sum_{n=-\infty}^{\infty} \frac{e^{-\lambda} I_n(\lambda)}{\lambda} \left[1 + \frac{\omega'}{\sqrt{2}\, k_\parallel U_t} Z(\xi') \right] = 0 \qquad (8)$$

where $\omega' = \omega - k_\parallel U_d$, the Doppler-shifted frequency, and

$$\xi' = \frac{\omega' - n\omega_c}{\sqrt{2}\, k_\parallel U_t} \quad .$$

Similarly, if $V_\parallel$ in Eq. (5) is replaced by $V_\parallel - U_d$, the corresponding dispersion equation is again given by Eq. (6), with ω replaced by $\omega' = \omega - k_\parallel U_d$.

4. Ambient Plasma Plus a Field-Aligned Stream

Let $D_p(\omega,\vec{k}) = 0$ be the dispersion equation for the ambient plasma--i.e., let $D_p(\omega,\vec{k})$ represent the left-hand side of any dispersion equation in the previous sections. If we let $D_s(\omega,\vec{k})$ be the dispersion function due to the stream, the overall dispersion equation of the system is then given by

$$D_p(\omega,\vec{k}) + D_s(\omega,\vec{k}) = 0 \quad . \tag{9}$$

To derive the expression $D_s(\omega,\vec{k})$, we assume that the distribution of the stream takes the form:

$$f_s(\vec{V}) = f_\perp(V_\perp)\ \delta\ (V_\parallel - U_s) \tag{10}$$

where U_s is the stream velocity along $\vec{B}_o$. Substituting Eq. (10) into the integral of Eq. (1) yields

$$D_s(\omega,\vec{k}) = \omega_s^2 \sum_{n=-\infty} \left[\frac{n\Omega_s}{\omega - k_\parallel U_s - n\Omega_s} I_1 - \frac{k_\parallel^2}{\omega - k_\parallel U_s - n\Omega_s} I_2 \right] \tag{11}$$

where ω_s = stream plasma frequency, Ω_s (carrying the sign of charge) = gyrofrequency of the particles in the stream, and I_1 and I_2 are given by

$$I_1 = 2\pi \int_0^\infty J_n^2(\chi_s)\, \frac{df_\perp}{dV_\perp}\, dV_\perp \quad ; \quad I_2 = 2\pi \int_0^\infty J_n^2(\chi_s)\, f_\perp V_\perp dV_\perp \tag{12}$$

where $\varkappa_s = k_\perp V_\perp / \Omega_s$.

For the case of a monoenergetic stream along the field line, f_s takes the form

$$f_s = \frac{1}{2\pi V_\perp} \delta(V_\perp)\ \delta(V_\parallel - U_b) \tag{13}$$

Integration of I_1, I_2 in Eq. (12) is then straightforward. Equation (11) can be reduced to the form:

$$D_s(\omega, \vec{k}) = \left[\frac{k_\parallel^2 \omega_s^2}{(\omega - k_\parallel U_b)^2} + \frac{k_\perp^2 \omega_s^2}{(\omega - k_\parallel U_b)^2 - \Omega_s^2} \right] \tag{14}$$

C. Ion Cyclotron Waves

In this section we examine the propagation characteristics of ion cyclotron waves in a stable plasma. For this purpose we assume that the electrons and ions exhibit an isotropic, stationary Maxwellian distribution, and we use the dispersion equation given by Eq. (3) or Eq. (4).

1. Collisionless Case

In the case of no collisions, the dispersion equation is given by Eq. (3). For the isotropic, stationary Maxwellian plasma, the wave modes contained in the dispersion equation consist of no instabilities. The wave may be subjected to Landau damping. In the linear regime, Landau damping is proportional to $\mathrm{Im}Z(\xi)$. (Im stands for the imaginary part.) For the wave propagating at a large angle with respect to $\vec{B}_o$ ($k_\parallel$ becomes small), $\mathrm{Im}Z(\xi)$ is then much smaller than $\mathrm{Re}Z(\xi)$, and the waves are substantially free of Landau damping. In the remainder of this section we shall discuss the three cases: $k_\parallel = 0$; $k_\perp = 0$; and $k_\perp \neq 0$, $k_\parallel \neq 0$, and $k_\perp \gg k_\parallel$.

a. $\underline{k_{\parallel} = 0}$

For this case, the propagation direction is exactly perpendicular to $\vec{B}_o (\vec{k}_{\perp} \vec{B}_o)$. In the following, we use the subscripts "e" and "i" to designate the parameters for the electrons and ions, respectively. Solving for ion cyclotron waves, we assume that

$$\frac{\lambda_e}{\lambda_i} = \frac{m_e}{m_i} \frac{T_e}{T_i} \ll 1 \tag{15}$$

which yields the approximation

$$I_n(\lambda_e) \exp - \lambda_n \simeq (1 - \lambda_e) \frac{\lambda_e^n}{2^n n!} \tag{16}$$

Using Eqs. (15) and (16) we can approximate Eq. (3) by the form:

$$1 - \frac{\omega_{pe}^2}{\omega^2 - \omega_{ce}^2} - \sum_{n=1}^{\infty} \frac{2n^2 \omega_{pi}^2}{\omega^2 - (n\omega_{ci})^2} \frac{I_n(\lambda_i)}{\lambda_i} \exp - \lambda_i = 0 \quad . \tag{17}$$

For the n^{th} ion cyclotron harmonic wave, $\omega^2 \simeq (n\omega_{ci})^2$, Eq. (17) yields

$$\omega^2 = (n\omega_{ci})^2 + \frac{2n^2 \omega_{pi}^2 \omega_{ce}^2}{\omega_u^2} \frac{I_n(\lambda_i)}{\lambda_i} \exp - \lambda_i \tag{18}$$

where $\omega_u^2 = \omega_{pe}^2 + \omega_{ce}^2$ and $n\omega_{ci} < \omega < (n+1)\omega_{ci}$.

Equation (18) can be plotted to yield the dispersion curves--i.e., plots of ω versus $k_{\perp}$ for each n and the other plasma parameters. From the ω-versus-$k_{\perp}$ plots, the phase velocity $\omega/k_{\perp}$ can be determined. Two limiting approximations can be made to simplify Eq. (19).

Approximation 1: $\lambda_i \ll 1$. In the case of phase velocity much larger than the ion thermal speed U_i, or wavelength much larger than the ion Larmor radius, we have $\lambda_i \ll 1$. Equation (18) can be approximated by

$$\omega^2 = (n\omega_{ci})^2 + \frac{n^2\omega_{pi}^2\omega_{ce}^2}{\omega_u^2}\left[\left(1 - \lambda_i\right)\left(\frac{\lambda_i}{2}\right)^{n-1}\right] . \tag{19}$$

Approximation 2: $\lambda_i \gg 1$. Reversing the limiting case discussed above, we use $I_n(x) \simeq (\exp x)/\sqrt{2\pi x}$. Equation (18) can then be approximated by

$$\omega^2 = (n\omega_{ci})^2 + \sqrt{\frac{2}{\pi}}\,\frac{n^2\omega_{pi}^2\omega_{ce}^2}{\omega_u^2}\left(\frac{\omega_{ci}}{k_\perp U_i}\right)^3 \tag{20}$$

b. $k_\perp = 0$

For the case of wave propagation exactly along the static magnetic field, the dispersion equation, Eq. (3), reduces to

$$k_z^2 - \frac{\omega_{pe}^2}{U_e^2}\left[1 + Z'(\xi)\right] - \frac{\omega_{pi}^2}{U_i^2}\left[1 + Z'(\xi_i)\right] = 0 \tag{21}$$

where $Z'(\xi) = \partial Z(\xi)/\partial\xi$.

It is seen that the cyclotron frequencies have disappeared from the dispersion equation. The solutions of Eq. (21) are simply the longitudinal plasma waves, which degenerate into plasma oscillation when Te = Ti = 0. Since the imaginary part of Z' is quite large, these plasma waves are subject to strong Landau damping.

c. $k_\perp \neq 0$, $k_\parallel \neq 0$, and $k_\perp \gg k_\parallel$

In this case, we consider that ion cyclotron waves propagate with large angle with respect to $\vec{B}_o$. Since $k_\parallel$ is small, ξ_e and ξ_i are much greater than unity. Thus the Landau damping can again be neglected. After some algebra, the dispersion equation can be reduced to

$$1 - \frac{\omega_{pe}^2 \sin^2\theta}{\omega^2 - \omega_{pe}^2} - \sin^2\theta \sum_{n=1}^{\infty} \frac{2n^2\omega_{pi}^2}{\omega^2 - n^2\omega_{ci}^2} \frac{I_n(\lambda_i)}{\lambda_i} \exp(-\lambda_i) = 0 \qquad (22)$$

where θ is polar angle between $\vec{B}_o$ and $\vec{k}$.

For n^{th} ion cyclotron harmonic waves, Eq. (22) yields

$$\omega^2 = n^2\omega_{ci}^2 + \frac{2n^2\omega_{pi}^2\omega_{ce}^2 \sin^2\theta}{\omega_{pe}^2 \sin^2\theta + \omega_{ce}^2} \frac{I_n(\lambda_i)}{\lambda_i} \exp(-\lambda_i) \qquad (23)$$

where $n\omega_{ci} < \omega < (n+1)\omega_{ci}$.

The asympotic forms for $\lambda_i \ll 1$ and $\lambda_i \gg 1$ are similar to that for the case of $k_\parallel = 0$, with the factor $\sin\theta$ multiplying ω_{ce} and ω_{pe} as indicated in Eq. (22).

2. Finite Collisions

When the effects of collisions cannot be neglected, the ion cyclotron waves are subject to collisional damping. The dispersion equation for ion cyclotron modes propagating perpendicular to $\vec{B}_o$ is now given by

$$D(\omega,\vec{k}) = 1 - \frac{\omega_{pe}^2(1 - j\tilde{\nu}_e)}{(\omega - j\nu_e)^2 - \omega_{ce}^2} - \sum_{n=1}^{\infty} \frac{2n^2\omega_{pi}^2(1 - j\tilde{\nu}_i)}{(\omega - j\nu_i)^2 - (n\omega_{ci})^2} \frac{I_n(\lambda_i)}{\lambda_i} \exp\left(-\lambda_i\right) = 0 \qquad (24)$$

where $\tilde{\nu}_e = \nu_e/\omega$, $\tilde{\nu}_i = \nu_i/\omega$.

To calculate the collisional damping rate we note that the propagation factor $\exp j(\omega t - \vec{k} \cdot \vec{x})$ is used. Thus, $\mathrm{Im}\omega$ (taking positive value) is the temporal damping rate. For the case of weak damping, $\mathrm{Im}\omega$ can be calculated by

$$\mathrm{Im}\omega = \frac{\mathrm{ImD}(\omega,\vec{k})}{\frac{\partial \mathrm{ReD}(\omega,\vec{k})}{\partial \omega}} \Bigg|_{\text{roots of } \mathrm{ReD}(\omega,\vec{k}) = 0} . \tag{25}$$

Using Eqs. (24) and (25) and omitting some algebra we obtain the following results for the collisional damping rate for n^{th} ion cyclotron harmonic waves, for $\nu_e = 0$:

$$\mathrm{Im}\omega = \frac{\nu_i(\nu_i^2 + 2n^2\omega_{ci}^2)(1 + 4n^2\tilde{\omega}_i)}{2n^2\omega_{ci}^2(4n^2\tilde{\omega}_i^2 - 1)} \tag{26}$$

and for $\nu_e \gg \nu_i$:

$$\mathrm{Im}\omega = \frac{\omega_{pe}^2 \nu_e}{2n^4\omega_{pi}^2\omega_{ce}^2\omega_{ci}^2} \frac{(\nu_i^4 + 4n^2\nu_i^2\omega_{ci}^2)^2}{(4n^2\nu_i^2\omega_{ci}^2 - \nu_i^4)} \frac{\lambda_i}{2I_n(\lambda_i)\exp(-\lambda_i)} \tag{27}$$

where $\tilde{\omega} = \omega_{ci}/\nu_i$, and where $\omega_{pe}^2 > \Omega_e^2 \gg \nu_e^2$ is assumed, and $\omega^2 \simeq n^2\omega_{ci}^2$ is used.

For the case of $k_\parallel \neq 0$, but small, it can be shown that the damping rate $\mathrm{Im}\omega$ is again given by Eqs. (26) and (27), since the term involving $\sin\theta$ is absent in the use of the approximation $\omega^2 \simeq n^2\omega_{ci}^2$.

D. Future Work

In previous sections we have presented a number of general forms of the dispersion equation under the various plasma conditions. For the case of a stable plasma, the dispersion equation has been solved for the ion-cyclotron harmonic waves. When the finite collisions are included, the formulas of the collisional damping rate for the ion cyclotron harmonic waves have also been derived.

As the next step, we should consider several models of unstable plasma in the auroral region, and investigate the instabilities of the ion cyclotron waves. With and without collisions, the onset (threshold) conditions for instability and the formulas of the growth rate should be derived.

It is expected that the above-mentioned quantities of the ion cyclotron waves are closely related to the field-aligned streams and currents. Thus, these results can be used not only to explain the Doppler spectra of auroral clutter, but also as a diagnostic tool to measure the field-aligned currents.

V DISCUSSION

It is clear from the results presented in this report that great strides have been made during the past 2 or 3 years toward an understanding of auroral-clutter production mechanisms. With the installation of both the 398-MHz phased-array radar at Homer and the incoherent-scatter radar at Chatanika, it became possible for the first time to continuously monitor the plasma parameters within a radar scattering volume producing auroral clutter. The combined use of the two radars together with other auroral/magnetospheric measurements has made it possible to evaluate existing plasma instability models as candidate scattering mechanisms and to determine auroral clutter characteristics that must be explained by any successful theory.

Recent results showed that the Buneman-Farley two-stream instability is still a prime candidate as the source of auroral clutter. However, it is now clear that while the two-stream primary waves may in fact be the driving force, auroral clutter is apparently not produced by direct backscatter from these irregularities. Evidence for the two-stream instability as the prime driving source is: (1) the existence of a threshold electric field strength of 30 mV/m;[15] and (2) Doppler velocity characteristics as related to the ion-acoustic speed,[7] the magnetic aspect angle,[7,32] and the current direction.[6,7]

The gradient-drift instability also remains a candidate, however, primarily through its role in the production of secondary plasma waves. In its linear form this instability appears incapable of producing scale sizes necessary to explain auroral clutter observed at frequencies as high as 3 GHz. The only model that allows for the generation of small-

size gradient-drift waves is still not completely satisfactory. As discussed by Tsunoda,[6] the ion velocity effects that appear in observed *Doppler-velocity data cannot* be accounted for by this theory. Furthermore, the necessary assumption that wave steepening does not occur appears to break down at large primary wavenumbers.[7]

The question of whether the ion-cyclotron instability might play a role in the production of auroral clutter or at least contribute to the modification of the observed echo characteristics remains to be investigated. The discovery that the diffuse auroral clutter (DB) found in the evening sector is collocated with downward field-aligned currents suggests the possibility that ion-cyclotron waves may be present. However, the fact that most of the downward field-aligned currents in the DB region are probably carried by upward-moving thermal electrons in the F region may negate this suggestion. There does remain the possibility that visual aurora and discrete auroral clutter are associated with ion-cyclotron waves.

The determination of microscale and macroscale relationships (see Section II) has also converted the backscatter radar into a valuable diagnostic tool for auroral and magnetospheric research.

The typical morphological features that can be extracted from the auroral clutter were presented in Section II (see Figure 2). Regions of enhanced electric fields and significant electron density are mapped by the auroral clutter. Both Doppler and amplitude characteristics of auroral clutter appear capable of providing quantitative information regarding the electric field and E-region current density.

A direct application of these morphological features is to test the NRL/DNA Auroral codes. The capabilities of the Homer (609) and Chatanika (617) radars have been extended so that they are able to monitor nearly all of the ionospheric plasma parameters that are the input and

output of the NRL/DNA Auroral codes. The only key parameter not presently measurable by the ground-based radars is the field-aligned current, which is monitored by a vector magnetometer on the Navy TRIAD satellite. (At least two other satellites are able to provide similar measurements--ISIS-2 and the Air Force S3-2.)

The principal outputs of the Auroral code are the magnitude and spatial variation of (1) the ionospheric electric field, (2) the electrojet currents, and (3) the net electric current flow parallel to the geomagnetic field line (field-aligned current). The 617 and 609 radars can measure the ionospheric electric field and electrojet currents as a function of latitude. At the present time it is not possible to measure field-aligned current with the ground-based systems.

The principal role of the Homer radar in such a coordinated experiment is illustrated in Figure 8. The Chatanika radar measurements are generally restricted to the region in or near the local geomagnetic meridian. The plane in which data are gathered by a satellite rarely, if ever, is coincident with the Chatanika meridian. Consequently, the two-dimensional (latitude, longitude) mapping capability of the 609 radar is the essential link between the 617 radar and TRIAD measurements. The sensitivity of the Homer radar to regions of enhanced electric field strengths and electrojet currents can be used to map these regions, allowing accurate spatial (and temporal) extrapolation between the planes of the TRIAD pass and the Chatanika radar measurements. Note in Figure 8 that by utilization of the mechanical steering capability of the Homer radar in addition to its 40^{o} electronic scan, the longitudinal coverage can be significantly extended.

In the course of the reported auroral clutter studies, related studies have shown that auroral clutter is probably not limited only to the auroral E region. Ott and Farley[33] recently developed a plasma

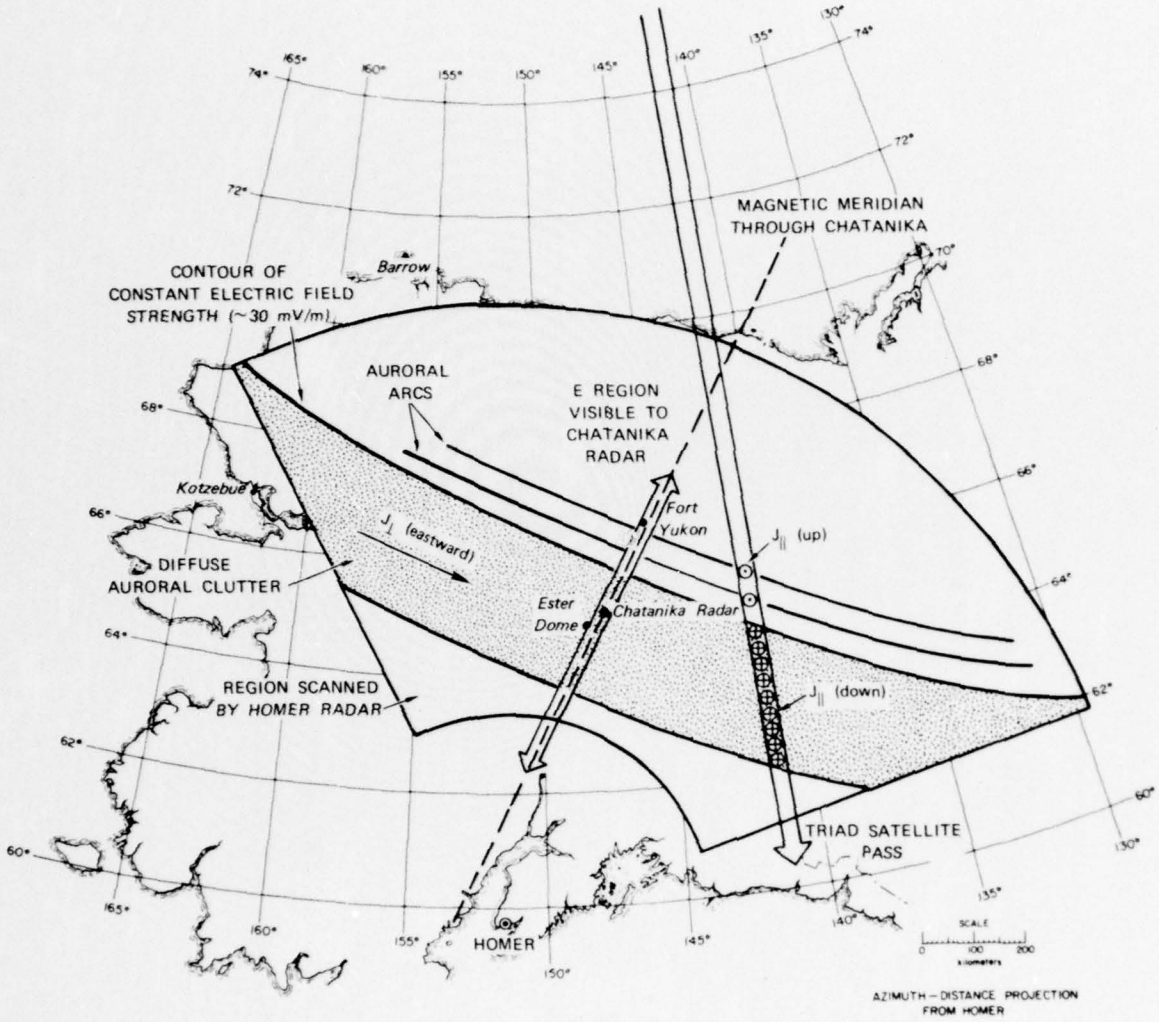

FIGURE 8 A TECHNIQUE FOR USING THE HOMER PHASED-ARRAY RADAR TO ALLOW ACCURATE EXTRAPOLATION BETWEEN SATELLITE MEASUREMENTS AND CHATANIKA RADAR MEASUREMENTS

instability model that predicts the generation of field-aligned irregularities in the auroral F region. The instability is based on an anisotropic ion velocity distribution brought about by charge-exchange processes in the F region. The driving force is again a large electric field ($\gtrsim$45 mV/m). The discovery of this instability is a prime example illustrating our still rather meager understanding of electric field effects and plasma instabilities.

The irregularities associated with this instability have apparently gone undetected by most auroral backscatter radars due to its field-aligned characteristics. Because of the geometry of the geomagnetic field at high latitudes, it is virtually impossible for ground-based radars to view the F region in directions nearly perpendicular to the field lines. However, there is experimental evidence that seems to confirm its existence. Leadabrand et al.[34] made auroral radar measurements at frequencies of 401 and 800 MHz that showed echoes up to an altitude of 160 km or so, which was the maximum height at which orthogonality was achieved. A second, non-auroral radar observation was made at 106.1 MHz from Stanford, California.[35] During periods of high magnetic activity when the auroral oval shifted to low latitudes, field-aligned echoes were observed to altitudes as high as 300 km. Although the instability proposed by Ott and Farley does not predict backscatter as low as 106 MHz, the observation clearly demonstrates that F-region auroral clutter does indeed occur.

VI CONCLUSIONS AND RECOMMENDATIONS

We have shown that auroral-clutter-producing mechanisms can be effectively studied through coordinated field experiments utilizing the Homer 609 radar, the Chatanika 617 radar, and other supporting measurements. Most of the results obtained to date pertained to diffuse auroral clutter. The choice of the diffuse auroral clutter for the initial study was based on its well-behaved spatial and temporal characteristics. In contrast, the discrete auroral clutter is characterized by a more complex and dynamic behavior, often associated with auroral substorm activity.

We have shown that diffuse auroral clutter is characterized by a threshold electric field strength of 30 mV/m. Diffuse auroral clutter was also shown to be collocated with regions of diffuse particle precipitation and of auroral electrojet flow. Evidence was also presented to indicate that the amplitude is probably proportional to the current density, in a manner similar to that observed at 50 MHz by Greenwald et al.[17,18] Both amplitude and Doppler characteristics were found to be generally consistent with the production of field-aligned irregularities by a plasma instability model not unlike that presented by Sudan et al.[13]

The discrete auroral clutter remains to be characterized. With the phased-array radar, it will be possible for the first time to characterize the discrete auroral clutter, in both amplitude and Doppler. The clutter-producing mechanism associated with the discrete echoes are believed to be similar to the field-aligned nuclear clutter observed due to beta ionization.

The new theoretical evidence that field-aligned F-region clutter can be expected when electric field strengths of the order of 50 mV/m or greater exist opens a new area of study pertinent to clutter environments. The theoretical results appear to be supported by at least two past experimental studies conducted by Stanford Research Institute.

Finally, advantage should be taken of the Homer and Chatanika radars to test the NRL/DNA Auroral codes. A discussion on how the Homer and Chatanika radars could be utilized to test the NRL/DNA Auroral codes was presented in Section V.

REFERENCES

1. W. G. Chesnut, J. C. Hodges, and R. L. Leadabrand, "Auroral Wavelength Dependence Studies," Final Report, Contract AF30(602)-3734, SRI Project 5535, Stanford Research Institute, Menlo Park, Calif. (June 1968).

2. W. G. Chesnut, J. C. Hodges, and R. L. Leadabrand, "Correlation of Radar Echoes from the Aurora with Satellite-Measured Auroral Particle Precipitation," Final Report, Contract DASA01-67-C-0066, DNA 2825F, SRI Project 6548, Stanford Research Institute, Menlo Park, Calif. (December 1971).

3. R. L. Leadabrand, M. J. Baron, J. Petriceks, and H. F. Bates, "Chatanika, Alaska, Auroral Zone Incoherent Scatter Facility," Radio Sci., Vol. 7, p. 747 (1972).

4. R. I. Presnell, "DNA Project 609 Radar: Auroral Backscatter Measurements," Final Report, Contract DNA001-72-C-0179, DNA 3307F, SRI Project 2001, Stanford Research Institute, Menlo Park, Calif. (April 1974).

5. M. J. Baron, "DNA Project 617 Radar: Auroral Ionospheric Measurements," Final Report, Contract DNA001-72-C-0076, DNA 3023F, SRI Project 1703, Stanford Research Institute, Menlo Park, Calif. (December 1972).

6. R. T. Tsunoda, "Electric Field Measurements Above a Radar Scattering Volume Producing 'Diffuse' Auroral Echoes," J. Geophys. Res., Vol. 80, p. 4297 (1975).

7. R. T. Tsunoda, "Doppler Velocity Maps of the Diffuse Radar Aurora," J. Geophys. Res., Vol. 81 (in press, 1976).

8. P. M. Banks, J. R. Doupnik, and S. -I. Akasofu, "Electric Field Observations by Incoherent Scatter Radar in the Auroral Zone," J. Geophys. Res., Vol. 78, p. 6607 (1973).

9. A. Brekke, J. R. Doupnik, and P. M. Banks, "A Preliminary Study of the Neutral Wind in the Auroral E Region," J. Geophys. Res., Vol. 78, p. 8235 (1973).

10. R. T. Tsunoda, R. I. Presnell, and R. L. Leadabrand, "Radar Auroral Echo Characteristics as Seen by a 398-MHz Phased-Array Radar Operated at Homer, Alaska," J. Geophys. Res., Vol. 79, p. 4709 (1974).

11. O. Buneman, "Excitation of Field-Aligned Sound Waves by Electron Streams," Phys. Rev. Lett., Vol. 10, p. 285 (1963).

12. D. T. Farley, "A Plasma Instability Resulting in Field-Aligned Irregularities in the Ionosphere," J. Geophys. Res., Vol. 68, p. 6083 (1963).

13. R. N. Sudan, J. Akinrimisi, and D. T. Farley, "Generation of Small-Scale Irregularities in the Equatorial Electrojet," J. Geophys. Res., Vol. 78, p. 240 (1973).

14. R. A. Greenwald, "Diffuse Radar Aurora and the Gradient-Drift Instability," J. Geophys. Res., Vol. 79, p. 4807 (1974).

15. R. T. Tsunoda and R. I. Presnell, "On a Threshold Electric Field Associated with the 398-MHz Diffuse Radar Aurora," J. Geophys. Res., Vol. 81, p. 88 (1976).

16. R. T. Tsunoda, R. I. Presnell, Y. Kamide, and S. -I. Akasofu, "Relationship of Radar Aurora, Visual Aurora, and Auroral Electrojets in the Evening Sector," submitted to J. Geophys. Res. (1976).

17. R. A. Greenwald, W. L. Ecklund, and B. B. Balsley, "Auroral Currents, Irregularities, and Luminosity," J. Geophys. Res., Vol. 78, p. 8193 (1973).

18. R. A. Greenwald, W. L. Ecklund, and B. B. Balsley, "Radar Observations of Auroral Electrojet Currents," J. Geophys. Res., Vol. 80, p. 3635 (1975).

19. D. D. Wallis, C. D. Anger, and G. Rostoker, "The Spatial Relationship of Auroral Electrojets and Visible Aurora in the Evening Sector," submitted to J. Geophys. Res. (1975).

20. O. de la Beaujardiere, M. J. Baron, and R. R. Vondrak, "Radar Observations of Electric Fields and Currents Associated with Auroral Arcs," presented at Fall AGU Meeting, San Francisco, Calif. (December 1975).

21. R. T. Tsunoda, R. I. Presnell, and T. A. Potemra, "The Spatial Relationship Between the Evening Radar Aurora and Field-Aligned Currents," accepted for publication, J. Geophys. Res. (1976).

22. A. T. Y. Lui and C. D. Anger, "A Uniform Belt of Diffuse Auroral Emission Seen by the ISIS-2 Scanning Photometer," Planet. Space Sci., Vol. 21, p. 799 (1973).

23. A. T. Y. Lui, P. Perreault, S. -I. Akasofu, and C. D. Anger, "The Diffuse Aurora," Planet. Space Sci., Vol. 21, p. 857 (1973).

24. Y. Kamide and S. -I. Akasofu, "The Location of the Field-Aligned Current with Respect to Discrete Arcs," accepted for publication, J. Geophys. Res. (1976).

25. P. D. Perreault and M. J. Baron, "ICECAP '74--Chatanika Radar Results," Technical Report 6, Contract DNA001-74-C-0167, SRI Project 3118, Stanford Research Institute, Menlo Park, Calif. (October 1975).

26. J. P. Heppner, "The Harang Discontinuity in Auroral Belt Ionospheric Currents," Geofys. Publ., Vol. 29, p. 105 (1972).

27. J. Minkoff, P. Kugelman, and J. Weissman, "Radio Frequency Scattering from a Heated Ionospheric Volume, 1, VHF/UHF Field-Aligned and Plasma-Line Backscatter Measurements," Radio Sci., Vol. 9, p. 941 (1974).

28. N. D'Angelo, "Type 3 Spectra of the Radar Aurora," J. Geophys. Res., Vol. 78, p. 3987 (1973).

29. B. B. Balsley and W. L. Ecklund, "VHF Power Spectra of the Radar Aurora," J. Geophys. Res., Vol. 77, p. 4746 (1972).

30. B. D. Fried and S. D. Conte, The Plasma Dispersion Function (Academic Press, New York, N.Y., 1961).

31. J. A. Tatronis and F. W. Crawford, "Cyclotron Harmonic Wave Propagation and Instabilities. II. Oblique Propagation," J. Plasma Phys., Vol. 4, pt. II, p. 249 (1970).

32. T. N. C. Wang and R. T. Tsunoda, "On a Crossed Field Two-Stream Plasma Instability in the Auroral Plasma," J. Geophys. Res., Vol. 80, p. 2172 (1975).

33. E. Ott and D. T. Farley, "Microinstabilities and the Production of Short-Wavelength Irregularities in the Auroral F Region," J. Geophys. Res., Vol. 80, p. 4599 (1975).

34. R. L. Leadabrand, J. C. Schlobohm and M. J. Baron, "Simultaneous Very High Frequency and Ultra High Frequency Observations of the Aurora at Fraserburgh, Scotland," J. Geophys. Res., Vol. 70, p. 4235 (1965).

35. J. C. Schlobohm, R. L. Leadabrand, R. B. Dyce, L. T. Dolphin, and M. R. Berg, "High-Altitude 106.1-Mc Radio Echoes from Auroral Ionization Detected at a Geomagnetic Latitude of 43°," J. Geophys. Res., Vol. 64, p. 1191 (1959).

DISTRIBUTION LIST

DEPARTMENT OF DEFENSE

Director
Defense Advanced Research Projects Agency
ATTN: Strategic Tech. Office
ATTN: Lieutenant Colonel W. A. Whitaker
ATTN: STO, Captain J. Justice
ATTN: Major Gregory Canavan

Director
Defense Communications Agency
ATTN: Code 480

Defense Documentation Center
12 cy ATTN: TC

Director
Defense Nuclear Agency
ATTN: RAAE, Major John Clark
ATTN: STSI, Archives
ATTN: RAAE, Harold C. Fitz, Jr.
ATTN: DDST
2 cy ATTN: STTL, Tech. Lib.
3 cy ATTN: RAAE
3 cy ATTN: RAAE, Charles A. Blank

Director of Defense Research & Engineering
ATTN: DDS&SS, Richard S. Ruffine
ATTN: AD/S&AS, Daniel Brockway
ATTN: AD/DS
ATTN: DD/S&SS, John B. Walsh

Commander
Field Command
Defense Nuclear Agency
ATTN: FCPR

Director
Interservice Nuclear Weapons School
ATTN: Doc. Con.

Chief
Livermore Division, Field Command, DNA
ATTN: FCPRL

Commander
National Military Command Sys. Support Center
ATTN: Deputy Director for CSPO

OJCS/J-3
ATTN: J-3, Ops. Anal. Br., Mr. Toma

DEPARTMENT OF THE ARMY

Commanding Officer
Atmospheric Sciences Laboratory
ATTN: E. Butterfield

Director
Ballistic Missile Defense Advanced Technical Center
ATTN: ATC-T, Melvin T. Capps
ATTN: CRDABH, O. W. Davies

Commander
TRASANA
ATTN: EAB

DEPARTMENT OF THE ARMY (Continued)

Program Manager
Ballistic Missile Defense Program Office
ATTN: DACS-BMS, Julian Davidson
ATTN: John Shea
ATTN: DACS-BMM

Commander
Harry Diamond Laboratories
ATTN: DRXDO-NP, Francis N. Wimenitz
2 cy ATTN: DRXDO-NP

Director
U.S. Army Ballistic Research Laboratories
ATTN: DRXBR-CA, Franklin E. Niles

Commander
U.S. Army Foreign Science & Tech. Center
ATTN: R. Jones
ATTN: P. A. Crowley

Commander
U.S. Army Materiel Dev. & Readiness Command
ATTN: DRCDE-D, Lawrence Flynn

Commander
U.S. Army Missile Command
ATTN: DRSMI-XS, Chief Scientist
ATTN: Chief, Doc. Sec.

Commander
U.S. Army Nuclear Agency
ATTN: USANUA, W. J. Berberet

DEPARTMENT OF THE NAVY

Chief of Naval Research
ATTN: Code 464, Jacob L. Warner
ATTN: Code 427, CDR Ronald J. Oberle
ATTN: Code 464, Thomas P. Quinn

Commander
Naval Air Systems Command
ATTN: AIR 5381

Commander
Naval Electronics Laboratory Center
ATTN: Code 2200, Ilan Rothmuller
3 cy ATTN: Code 2200, Verne E. Hildebrand

Director
Naval Research Laboratory
ATTN: Code 7750, Darrell F. Strobel
ATTN: Code 7720, Edgar A. McClean
ATTN: Code 2027, Tech. Lib.
ATTN: Code 7127, Charles Y. Johnson
ATTN: Code 7701, Jack D. Brown
ATTN: Code 7750, Paul Juluenne
ATTN: Code 7750, Timothy P. Coffey
ATTN: Douglas P. McNutt

Commander
Naval Surface Weapons Center
ATTN: Code WX-21, Tech. Lib.
ATTN: Code WA-501, Navy Nuc. Prgms. Off.

DEPARTMENT OF THE NAVY (Continued)

Director
Strategic Systems Project Office
ATTN: NSP-2141
ATTN: NSP-27231, Marcus Meserole

DEPARTMENT OF THE AIR FORCE

Commander
ADC/DC
ATTN: DC, Mr. Long

Commander
ADC/XP
ATTN: XPQDQ, Maj G. Kuch

Commander
Aeronautical Systems Division, AFSC
ATTN: ASD-YH-EX, Lt Col Robert Leverette

AF Geophysics Laboratory, AFSC
ATTN: OPR, Hervey P. Gauvin
ATTN: LIR, T. J. Elkins
ATTN: LI
6 cy ATTN: OPR, James C. Ulwick
ATTN: OPR, Alva T. Stair
ATTN: LKB, Kenneth S. W. Champion
ATTN: OP, John S. Garing
ATTN: OPR

AF Weapons Laboratory, AFSC
ATTN: DYT, Maj Don Mitchell
ATTN: CA, Arthur H. Guenther
ATTN: DYT, Capt David W. Goetz
ATTN: SUL
ATTN: SAS, John M. Kamm

AFTAC
ATTN: TF, Maj E. Hines
ATTN: TF, Maj Wiley
ATTN: TN

HQ USAF/RD
ATTN: RDQ

Commander
Rome Air Development Center, AFSC
ATTN: EMTLD, Doc. Lib.
ATTN: V. Coyne

SAMSO/MN
ATTN: MNX

SAMSO/SZ
ATTN: SZJ, Maj Lawrence Doan

Commander in Chief
Strategic Air Command
ATTN: XPFS, Maj Brian G. Stephan

ENERGY RESEARCH & DEVELOPMENT ADMINISTRATION

Division of Military Application
U.S. Energy Research & Development Administration
ATTN: Doc. Con. for Major D. A. Haycock

University of California
Lawrence Livermore Laboratory
ATTN: Terry R. Donich, L-96

ENERGY RESEARCH & DEVELOPMENT ADMINISTRATION (Continued)

EG&G, Inc.
Los Alamos Division
ATTN: James L. Walker
ATTN: James R. Breedlove
ATTN: J. H. M. Fu

Los Alamos Scientific Laboratory
ATTN: Doc. Con. for R. A. Jeffries
ATTN: Doc. Con. for John S. Malik
ATTN: Doc. Con. for Herman Hoerlin
ATTN: Doc. Con. for R. F. Taschek
ATTN: Doc. Con. for Eric Jones

Sandia Laboratories
ATTN: Doc. Con. for W. D. Brown
ATTN: Doc. Con. for A. Dean Thornbrough
ATTN: Doc. Con. for Charles Williams
ATTN: Doc. Con. for J. C. Eckhardt, Org. 1250
ATTN: Doc. Con. for Clarence R. Mehl, Org. 5230
ATTN: Doc. Con. for 3141, Sandia Rpt. Coll.

OTHER GOVERNMENT AGENCIES

Department of Commerce
National Oceanic & Atmospheric Administration
ATTN: R-43, Donald J. Williams

Department of Commerce
Office of Telecommunications
ATTN: William F. Utlaut
ATTN: Glenn Falcon

DEPARTMENT OF DEFENSE CONTRACTORS

Aerodyne Research, Inc.
ATTN: F. Bien
ATTN: M. Camac

Aeronomy Corporation
ATTN: S. A. Bowhill

Aerospace Corporation
ATTN: G. W. Anderson
ATTN: V. Josephson
ATTN: T. Taylor
ATTN: R. Grove
ATTN: Harris Mayer
ATTN: Wallis Grabowsky
ATTN: R. D. Rawcliffe

Analytical Systems Engineering Corporation
ATTN: Radio Sciences

The Boeing Company
ATTN: Glen Keister

Brown Engineering Company, Inc.
ATTN: David L. Lambert, M.S. 18
ATTN: N. Passino

Calspan Corporation
ATTN: Romeo A. DeLiberis

University of Denver
ATTN: Sec. Officer for David Murcray
ATTN: Sec. Officer for Mr. Van Zyl

DEPARTMENT OF DEFENSE CONTRACTORS (Continued)

ESL, Inc.
ATTN: James Marshall

General Electric Company
Space Division
ATTN: M. H. Bortner, Space Sci. Lab.
ATTN: Robert H. Edsall

General Electric Company
TEMPO-Center for Advanced Studies
ATTN: Warren S. Knapp
ATTN: DASIAC
5 cy ATTN: DASIAC, Art Feryok

General Electric Company
ATTN: George H. Millman

General Research Corporation
ATTN: John Boys
ATTN: John Ise, Jr.
ATTN: Peter Redmond

Geophysical Institute
ATTN: T. N. Davis
ATTN: Neal Brown
ATTN: Tech. Lib.

Honeywell, Incorporated
ATTN: W. Williamson

HSS, Inc.
ATTN: Donald Hansen

Information Science, Inc.
ATTN: Walter F. Dudziak

Institute for Defense Analyses
ATTN: Joel Bengston
ATTN: Hans Wolfhard
ATTN: Ernest Bauer

IRT Corporation
ATTN: E. dePlomb

Johns Hopkins University
Applied Physics Laboratory
ATTN: Document Librarian

Kaman Sciences Corporation
ATTN: F. G. Foxwell

Lockheed Missiles & Space Company
ATTN: Robert D. Sears, Dept. 52-14
ATTN: J. B. Reagan, Dept. 52-12
ATTN: Tom James
ATTN: Richard G. Johnson, Dept. 52-12
ATTN: John B. Cladis, Dept. 52-12
ATTN: John Kumer
ATTN: Martin Walt, Dept. 52-10
ATTN: Robert H. Au
ATTN: Billy M. McCormac, Dept. 52-14

M.I.T. Lincoln Laboratory
ATTN: J. V. Evans
ATTN: Lib. A-082 for David M. Towle

Martin Marietta Aerospace
Orlando Division
ATTN: Roy W. Heffner

DEPARTMENT OF DEFENSE CONTRACTORS (Continued)

McDonnell Douglas Corporation
ATTN: Robert W. Halprin

Mission Research Corporation
ATTN: D. Archer
ATTN: Conrad L. Longmire
ATTN: Dave Sowle
ATTN: Ralph Kilb
ATTN: Gary McCarter
ATTN: P. Fischer
ATTN: M. Scheibe

The Mitre Corporation
ATTN: Bill Mehuron

North Carolina State University at Raleigh
ATTN: Sec. Officer for Walter A. Flood

Photometrics, Inc.
ATTN: Irving L. Kofsky

Physical Dynamics, Inc.
ATTN: Joseph B. Workman
ATTN: A. Thompson

Physical Sciences, Inc.
ATTN: Kurt Wray

The Trustees of Princeton University
ATTN: F. W. Perkins, Plasma Physics Lab.

R & D Associates
ATTN: R. P. Turco
ATTN: Forest Gilmore
ATTN: H. A. Ory
ATTN: Robert E. LeLevier
ATTN: Richard Latter

R & D Associates
ATTN: Herbert J. Mitchell

The Rand Corporation
ATTN: James Oakley
ATTN: Cullen Crain

Raytheon Company
ATTN: G. D. Thome

RCA Corporation
Government & Commercial Systems
ATTN: Tech. Lib.
ATTN: R. D. Bachinshy

Riverside Research Institute
ATTN: R. Popolow

Science Applications, Inc.
ATTN: Robert W. Lowen
ATTN: Daniel A. Hamlin
ATTN: Lewis M. Linson
ATTN: D. Sachs

Space Data Corporation
ATTN: Edward F. Allen

Stanford Research Institute
ATTN: Warren W. Berning

DEPARTMENT OF DEFENSE CONTRACTORS (Continued)

Stanford Research Institute
ATTN: Ray L. Leadabrand
ATTN: M. Baron
ATTN: Walter G. Chesnut
ATTN: Robert S. Leonard
ATTN: F. J. Fremouw
ATTN: L. L. Cobb
ATTN: R. T. Tsunoda
ATTN: R. I. Presnell
ATTN: T. N. C. Wang
50 cy ATTN: Personnel

Stanford Research Institute
ATTN: Dale H. Divis

Technology International Corporation
ATTN: W. P. Boquist

DEPARTMENT OF DEFENSE CONTRACTORS (Continued)

Thiokol Chemical Corp. Astro Met Site
ATTN: G. C. Alford

Utah State University
ATTN: Doran Baker
ATTN: C. Wyatt
ATTN: Kay Baker
ATTN: D. Burt

Visidyne, Inc.
ATTN: William Reidy
ATTN: T. C. Degges
ATTN: J. W. Carpenter